NASA TECHNICAL NOTE

NASA TN D-8349 c.1

NASA TN D-8349

FLIGHT LOADS MEASUREMENTS OBTAINED FROM CALIBRATED STRAIN-GAGE BRIDGES MOUNTED EXTERNALLY ON THE SKIN OF A LOW-ASPECT-RATIO WING

Clinton V. Eckstrom

Langley Research Center
Hampton, Va. 23665

NATIONAL AERONAUTICS AND SPACE ADMINISTRATION • WASHINGTON, D. C. • DECEMBER 1976

1. Report No. NASA TN D-8349	2. Government Accession No.	3. Recipient's Catalog No.
4. Title and Subtitle FLIGHT LOADS MEASUREMENTS OBTAINED FROM CALIBRATED STRAIN-GAGE BRIDGES MOUNTED EXTERNALLY ON THE SKIN OF A LOW-ASPECT-RATIO WING		5. Report Date December 1976
		6. Performing Organization Code
7. Author(s) Clinton V. Eckstrom		8. Performing Organization Report No. L-10904
		10. Work Unit No. 505-02-22-01
9. Performing Organization Name and Address NASA Langley Research Center Hampton, VA 23665		11. Contract or Grant No.
		13. Type of Report and Period Covered Technical Note
12. Sponsoring Agency Name and Address National Aeronautics and Space Administration Washington, DC 20546		14. Sponsoring Agency Code

15. Supplementary Notes

16. Abstract

Flight-test measurements of wingloads (shear, bending moment, and torque) were obtained by means of strain-gage bridges mounted on the exterior surface of a low-aspect-ratio, thin, swept wing which had a structural skin, full-depth honeycomb core, sandwich construction. Details concerning the strain-gage bridges, the calibration procedures used, and the flight-test results are presented along with some pressure measurements and theoretical calculations for comparison purposes.

17. Key Words (Suggested by Author(s))		18. Distribution Statement	
Flight testing Flight loads Low-aspect-ratio wing		Unclassified – Unlimited Subject Category 05	
19. Security Classif. (of this report) Unclassified	20. Security Classif. (of this page) Unclassified	21. No. of Pages 58	22. Price* $4.25

*For sale by the National Technical Information Service, Springfield, Virginia 22161

FLIGHT LOADS MEASUREMENTS OBTAINED FROM CALIBRATED STRAIN-GAGE BRIDGES MOUNTED EXTERNALLY ON THE SKIN OF A LOW-ASPECT-RATIO WING

Clinton V. Eckstrom
Langley Research Center

SUMMARY

Flight-test measurements of structural loads (shear, bending moment, and torque) were made at three spanwise stations on a low-aspect-ratio, thin, swept wing which had a structural skin, full-depth honeycomb core, sandwich construction. The measurements were made by using strain-gage bridges mounted on the external surface of the wing. Linear regression analysis was used to establish the relationship between loads applied during single-point calibration loadings and the measured electrical output of the strain-gage bridges. The established relationships are expressed by load equations applicable to each of three wing semispan stations for axis systems oriented parallel and perpendicular to the vehicle center line. The flight test was performed with a drone aircraft equipped with a large external fuel tank located beneath the fuselage in the area of the wing. During the flight test, this fuel tank was jettisoned. Therefore, the aircraft is considered to have two configurations, that is, external fuel tank on or external fuel tank off. For each configuration, there is essentially a linear relationship between wing structural load ratios and the aircraft angle of attack.

The wing structural loads (as determined from the strain-gage bridge measurements) were in close agreement with those determined from differential pressure measurements but were higher, in most cases, than theoretical estimates based on an aerodynamic finite-element analysis method.

INTRODUCTION

Calibrated strain-gage bridges have been used extensively to determine flight loads (shear, bending moment, and torque) on a variety of aircraft structures. For structures such as high-aspect-ratio wings with a spar-rib construction, the load paths between the wing and the fuselage are easily defined, and suitable methods of locating and calibrating the strain-gage bridges have been established (ref. 1). For low-aspect-ratio wings with multiple spars, the loads from the wing are carried into the fuselage at several places, and the problems of locating and calibrating strain-gage bridges for load measurements become more complex (refs. 2, 3, and 4).

The use of strain-gage bridges for load measurements on low-aspect-ratio wings of structural skin, honeycomb core, sandwich construction introduces additional complications because there are no easily identifiable structural load paths on which to locate the strain-gage bridges. (For wings constructed with spars and ribs, the strain gages for the shear and bending-moment bridges are usually mounted on the spar vertical webs and flanges, respectively (ref. 1).) Reference 5 presents details on the use of four strain-gage bridges mounted on the exterior surface to measure flight loads on this type of low-aspect-ratio wing. The measurements presented in reference 5 are for a single inboard station with the reference axis system oriented parallel and perpendicular to the wing 40-percent chord line.

This report presents the results of a more detailed study of a wing identical to that of reference 5. The evaluation presented here is based on a larger number of exterior surface mounted strain-gage bridges and a more extensive loads calibration procedure.

Flight loads measurements are presented for three wing semispan stations for axis systems oriented parallel and perpendicular to the aircraft center line as discussed in the appendix of reference 5. The wing reported on herein was also instrumented to measure differential pressures on the wing semispan opposite to that containing the strain-gage bridges. The results for the differential pressures measured during the flight test are reported in detail in reference 6; however, in this paper, some wingloads determined from integration of differential pressure measurements are presented and compared with those obtained from the strain-gage bridges.

SYMBOLS

Values are given in SI Units. The measurements and calculations were made in U.S. Customary Units.

c	chord
g	acceleration due to gravity, 9.80 m/sec^2
L_i	ith general load (that is, V, M, and T for each wing station)
M	bending moment, N-m
q_∞	free-stream dynamic pressure, Pa (In figs. 8, 9, and 12, q is used.)
T	torque, N-m

V	shear, N
X,Y	reference axes (fig. 3)
α	angle of attack, deg
β_{ij}	coefficient of jth bridge for ith load equation, Load/mV
μ_j	output of jth bridge, mV

Subscripts and abbreviations:

B	bending-moment bridge
T	torque bridge

WING AND INSTRUMENTATION

Wing

The low-aspect-ratio, thin, swept wing on which the flight loads measurements were obtained is the standard wing for the BQM-34E drone aircraft (supersonic Firebee II) shown in figure 1. The wing structure consists of upper and lower tapered thickness stainless steel skins which are bonded to a full-depth aluminum honeycomb core (there are no internal spar or rib-type structures in the wing). The wing has an aspect ratio of 2.5, a taper ratio of 0.3, a leading-edge sweep angle of 53°, and a maximum thickness of 3 percent of the chord length. The wing has no control surfaces and no incidence angle, dihedral angle, twist, or camber. The airfoil is an NACA 65-003 shape that has been modified to provide a finite thickness trailing edge. The wing has a span of 2.720 m, a reference area of 2.970 m^2, a net exposed area of 2.150 m^2, a projected center line root chord of 1.676 m, and a tip chord of 0.503 m. The total wing structure, including the fuselage crossover section, has a mass of approximately 67 kg.

Strain-Gage Bridges

The left semispan of the test wing was instrumented with strain-gage bridges mounted on the exterior surfaces at 11 locations (two at each location) as shown in figures 2 and 3. The bridges consisted of four strain gages each with each gage connected as an active arm in a Wheatstone bridge circuit. One bridge at each location was mounted entirely on the wing upper surface, with the four strain gages positioned in an X-pattern (see inset in fig. 2) so as to be sensitive primarily to skin shearing strains produced by torque loads. The bridges arranged in the X-pattern are identified by their location number (fig. 3) and by the addition of a letter T for torque bridge. The second bridge at each location consisted of two parallel gages on the upper surface and an identical set of two gages on the lower surface. These gages are arranged to be responsive to bending-moment loads (that is, compressive strain on the upper surface and tension strain on the lower surface for positive loads), they are identified by their location number and by the addition of a letter B for bending-moment bridge. Because of the sandwich construction of the wing, it was not possible to include bridges arranged in the usual manner for sensing shear loads as on a spar vertical web.

Axis Systems

The axis system for each strain-gage bridge station is oriented parallel and perpendicular to the vehicle center line as shown in figure 3. The X-axis for each semispan station passes through the respective sets of strain-gage bridges for that station. The Y-axes, which are coincident in orientation, pass through the intersection of the quarter chord line and the X-axis for the inboard station.

CALIBRATION PROCEDURE

The wing calibration procedure, which was performed prior to the flight test, consisted of applying calibration loadings to the wing and measuring the electrical imbalance, or output, of the strain-gage bridges. A regression analysis was then used, as explained in reference 1, to establish a relationship between the strain-gage bridge outputs and the wingloads shear (V), bending moment (M), and torque (T) resulting from the applied calibration loadings.

The relationship between wingloads and the strain-gage bridge outputs was established by using data from single-point calibration loadings. The accuracy of the established relationship was then checked by use of data from multipoint calibration loadings.

Calibration Loadings and Measured Bridge Outputs

Single-point loads.- Single-point calibration loadings were applied to the wing at each of the 15 calibration load point locations shown by the circles in figure 3, and the electrical output of each of the strain-gage bridges was recorded for that loading. To accomplish these loadings, the test wing was mounted on a drone aircraft fuselage, and the whole assembly was inverted (fig. 4) so that the applied loads (inert weights) would produce stresses similar in direction to upward flight loads. The large diameter inert weights were placed on sponge rubber pads, 0.05 m by 0.05 m, to achieve the loading without inducing high local stress concentrations. Calibration loads of 1246 N were applied at load point locations 1 to 5; loads of 890 N at load point locations 6 to 10; and loads of

445 N at load point locations 11 to 15. These loads were applied in 25-percent increments from zero to the maximum value and removed in the same manner. The bridge outputs measured were then plotted as a function of applied load as a check to evaluate scatter and to insure that the bridge response was linear for all bridges and for all load points. The least-squares method was used to fit a straight line to the bridge output data. The slope of this line was used to calculate the bridge output for the maximum loading where it was assumed that the bridge output was zero for zero load.

The calculated bridge output values are presented in tables I, II, and III, as are the associated shear, bending-moment, and torque loads for the inboard, midwing, and outboard strain-gage stations, respectively. The shear loading is the same as the applied calibration load as long as the calibration load is applied outboard of the wing station of interest. Bending-moment loads are the product of the applied load and the y-distance from the point of load application to the wing station of interest. Torque loads are the product of the applied load and the x-distance to the point of load application. For the noninverted aircraft, loads applied upward on the wing outboard of the strain-gage bridge station of interest result in positive shear and positive bending-moment loads. Torque loads are considred positive if they produce an aircraft nose-down moment about the Y-axis. Calibration loads applied at load points inboard of the wing station of interest are considered as zero wingloads; however, the associated strain-gage bridge outputs were recorded as shown in tables II and III and are used in the appropriate regression analysis.

In general, for calibration loads applied outboard of the strain-gage bridge of interest, the bending-moment bridges responded with positive outputs, and the torque bridges responded with negative outputs. Notable exceptions to this pattern were the responses of bridges 4B and 5B to calibration loads applied at load points 3, 4, and 5, the responses of bridge 8B to loads at points 8, 9, and 10, and the responses of bridge 11B to loads at points 11 to 15. All these strain-gage bridges are located on the aft portion of the wing and possibly are affected by the notch or discontinuity at the inboard edge where the fuselage crossover section of the wing is much shorter in chord length than the exposed portion of the wing.

Multipoint loads.- The calibration procedure also included the application of multipoint loadings to the wing in two patterns of five load locations each. The first pattern (set A) used load point locations 1, 3, 6, 8, and 11, and the second pattern (set B) used load point locations 2, 4, 6, 10, and 12. Calibration loads were applied in increments of 667 N at locations 1, 2, 3, and 4, 445 N at locations 6, 8, and 10, and 222 N at locations 11 and 12. The maximum multipoint wing loading of 4893 N occurred when two increments of calibration load were applied at each load point location in the pattern. The loading step, the incremental applied load and its location, the resultant wing loadings, and the measured bridge outputs for these multipoint loadings are presented in tables IV to IX.

Load Equations

Load equations which give the applied wing loadings in terms of the output of selected strain-gage bridges were determined by means of the regression analysis method described in references 1 and 5. These load equations have the form:

$$L_i = \begin{bmatrix} \beta_{11} & \beta_{12} & \beta_{13} & \cdot & \cdot & \cdot & \beta_{1j} \\ \beta_{21} & \beta_{22} & \beta_{23} & \cdot & \cdot & \cdot & \beta_{2j} \\ \cdot & \cdot & \cdot & \cdot & \cdot & \cdot & \cdot \\ \cdot & \cdot & \cdot & \cdot & \cdot & \cdot & \cdot \\ \cdot & \cdot & \cdot & \cdot & \cdot & \cdot & \cdot \\ \beta_{i1} & \beta_{i2} & \beta_{i3} & \cdot & \cdot & \cdot & \beta_{ij} \end{bmatrix} \begin{Bmatrix} \mu_1 \\ \mu_2 \\ \mu_3 \\ \cdot \\ \cdot \\ \cdot \\ \mu_j \end{Bmatrix}$$

where β_{ij} is the coefficient of the jth bridge for the ith load, and μ_j is the output of the jth bridge.

The regression analysis from which the coefficients β_{ij} are obtained can be performed using only one or as many of the available strain-gage bridges at each wing station as is desired. The regression analysis provides two statistical numbers which are useful in establishing which strain-gage bridge outputs should be used. One of these statistical numbers is the probable error of estimate of load. This number is essentially a measure of the scatter in the relationship between the selected strain-gage bridge outputs and the applied structural loads. The other statistical number is the estimate of probable error in each load coefficient. This value can be used to check for the inclusion of irrelevant or redundant bridges. In the initial evaluation it was observed that if a large number of strain-gage bridges were used, the probable error for the estimates of structural loads would be small but that the probable error for most of the load coefficients would be large. Large probable errors for load coefficients indicate the use of redundant strain-gage bridges. Generally, the use of more than three strain-gage bridges resulted in excessively large errors associated with one or more of the load coefficients.

For the single-point loading conditions (tables I, II, and III), load equations were derived for all possible combinations of one, two, and three strain-gage bridges for each of the strain-gage bridge semispan stations. (Bridges 11B and 11T at the outboard station were eliminated from consideration because of a limit on the number of telemetry channels available.) The resulting equations (175 combinations for the inboard station, 41 combinations for the midwing station, and 14 for the outboard station) were evaluated by using the probable error of the coefficients and the probable error of the estimates of the loads as criteria. The equations were also evaluated for their prediction of multipoint wing-loading conditions for loading steps 6 to 15 of both set A and set B multipoint loading calibrations. The capability of the equations to predict the selected multipoint loading conditions is summarized in table X. The strain-gage bridges selected for use in each load measurement equation, the load coefficients established from the single-point load calibration, the associated probable errors for coefficients and estimates of loads, and the range of accuracy with which the equations could estimate the 20 selected multipoint loading conditions are presented in table XI.

Inboard strain-gage bridge station.- The wingloads at the inboard station can be measured more accurately for bending moment than for shear or torsion for this wing structure and for the arrangement of strain-gage bridges used. This capability is evidenced by the large number of combinations of bridges which can estimate multipoint bending-moment loading conditions accurately (table X) and the small probable error of load estimate for the bridge combination selected (table XI). The probable error of load estimate for the moment equation is less than ±1 percent of the average applied calibration bending-moment load, and the selected equation was capable of estimating the bending moment loads applied during the multipoint loadings to within ±3 percent.

For the torque load equation, the probable error of load estimate is ±6 percent of the average applied calibration torque loading. The measured range of accuracy is slightly better at ±5 percent.

For the shear load equation, the probable error of load estimate is ±10 percent of the average applied calibration shear loading, and the measured range of accuracy is also ±10 percent. This reduction in accuracy is not surprising since it was not possible to arrange strain-gage bridges specifically for the measurement of shear load as can be done for more conventional spar-stringer-rib structures.

Midwing strain-gage bridge station.- At the midwing station, the equation for determining bending-moment loads is again the most accurate as judged by both the probable error criteria and the measured range of accuracy. The probable error of load estimate is ±5 percent of the average applied calibration bending-moment load, and the measured range of accuracy is ±6 percent.

The equation for determining shear loads exhibited the same measured range of accuracy as for the inboard station (±10 percent). However, the probable error of the load estimate is much larger at ±19 percent of the average applied calibration shear load. The equation for determining torque loads has a probable error of estimate of ±17 percent of the average applied calibration torque load and a measured range of accuracy of ±14 percent.

Outboard strain-gage bridge station.- At the outboard station, the equation for determining torque load is the most accurate when evaluated by both the probable error criteria and the measured range of accuracy. The probable error of load estimate for the torque equation is ±5 percent of the average applied calibration torque load, and the measured range of accuracy is ±7 percent. The probable errors of load estimate for the shear and bending-moment loads are ±45 percent and ±5 percent of the average applied calibration shear and bending-moment loads, respectively. The measured range of accuracy of each equation is ±13 percent.

There is some concern about the adequacy of the calibration procedure used for the outboard station. Reference 1 states that the calibration loads should be applied at various chordwise and spanwise locations. As shown in figure 3, there are five or more variations in location of calibration load points in the chordwise direction for each strain-gage bridge station. However, there is less variation in calibration load point locations in the spanwise direction. For the outboard strain-gage bridge station, all five calibration load points are located at the same spanwise station. Because there was no variation in the spanwise location of the applied calibration loads, the calibration for the outboard station is considered inadequate for shear and bending-moment loads, and the accuracies presented for these loads for the outboard station are considered questionable.

FLIGHT TEST

The instrumented wing was flight-tested on the Firebee II aircraft by personnel at the U.S. Naval Air Missile Test Center, Pt. Mugu, California. The flight was initiated by by a rocket-assisted ground launch similar to the arrangement shown in figure 5. The flight consisted of climbs, straight and level cruise, dives, pullups, and sustained, constant-altitude coordinated turns at aircraft normal load factors ranging from 2g to 6g.

The drone aircraft was equipped with a large jettisonable fuel tank located beneath the fuselage in the area of the wing (see fig. 1). The initial aircraft mass was 1002 kg including 157.4 kg of fuel in the external tank and 119.3 kg of fuel in the fuselage tank. The jettisonable external fuel tank had a mass of 28.8 kg. The total wing structure, as shown in figure 2, had a mass of approximately 67 kg with no fuel or other added mass in the wing. Useful test data were acquired over a Mach number range of 0.25 to 0.95 with the aircraft in the external-fuel-tank-on configuration and from 0.70 to 1.25 in the external-fuel-tank-off configuration. The data for the tank-on configuration are all in the subsonic range because the drone aircraft is limited to subsonic flight until after the external fuel tank is jettisoned. The drone aircraft flight was terminated by parachute recovery with final recovery being accomplished by a helicopter with a mid-air retrieval system (MARS). A photograph of the helicopter with the recovered drone aircraft is presented in figure 6. Information relating to the preparation for and the conduct of a similar flight test is presented in reference 7.

Drone aircraft performance data and wing instrumentation measurements (differential pressure transducer and strain-gage bridge outputs) were telemetered to ground receiving stations using an FM/FM telemetry system. The aircraft performance data were monitored on a continuous basis, whereas the wing instrumentation data were commutated at a rate of 30 samples per second. Sample data records for a portion of the flight are presented in figure 7 to show how the measurements varied with time during a turn maneuver.

Flight measurements of wing structural loads are presented in this report as a function of onboard measurements of aircraft angle of attack, flight Mach number, and free-stream dynamic pressure. A vane-type sensor mounted on the nose boom (see fig. 1) measured the angle of attack with respect to the horizontal reference plane of the aircraft. Static and total pressures were measured by the side-mounted pitot static tube from which Mach number and impact pressure were determined by an onboard air data computer. These measurements, as recorded at the ground telemetry receiving stations, are considered accurate to ± 0.04 for Mach number, ± 3.4 kPa for impact pressure, and $\pm 0.6^{\circ}$ for angle of attack in the subsonic Mach number range ($\leqq 0.95$) to $\pm 1.1^{\circ}$ in the transonic and supersonic Mach number range (>0.95). (These estimates of error include considerations of position error, instrument error, and telemetry error as applicable.) Dynamic pressures were calculated during the data reduction process by using the measured values of Mach number and impact pressure as inputs. During the flight test, when telemetry accuracy was included, the strain-gage bridge measurements were accurate from 0.05 to 0.15 mV depending on the measurement range for each bridge. The strain-gage bridge output measurements recorded during the calibration procedures are considered accurate to ± 0.003 mV.

RESULTS AND DISCUSSION

Wing structural loads measurements were obtained during the flight test by means of the calibrated strain-gage bridges on the left wing of the aircraft. These results are presented in figures 8 and 9. Figures 8 and 9 also show, for a few selected test conditions, wing loads as determined from integration of differential pressure distributions measured on the right wing. Theoretical predictions of wing structural loads for the external-fuel-tank-off aircraft configuration are also shown in the appropriate figures. Although direct comparisons between measured and theoretical results are made, this report does not evaluate any differences which may exist. Details of the results obtained are presented in the following sections.

Wingloads From Strain-Gage Bridge Measurements

The load coefficients presented in table X were used with the bridge outputs measured during the flight test to determine the wing structural loads; i.e., shear (V), bending moment (M), and torque (T). These measured loads are presented in figure 8 for the external-fuel-tank-on aircraft configuration and in figure 9 for the external-fuel-tank-off aircraft configuration. The wing structural loads are presented as a ratio to the instantaneous free-stream dynamic pressure and as a function of aircraft angle of attack for various Mach number regions for the inboard, midwing, and outboard strain-gage bridge stations. The data symbols shown represent measurements taken at a rate of one to six samples per second. For both aircraft configurations (that is, tank-on or tank-off), there is essentially a linear relationship between the measured wing structural load ratios and the aircraft angle of attack (over the test range of angles of attack) for each of the Mach number ranges shown. The straight line represents the best fit to the data using a least-squares analysis method. The number of samples included and the dynamic pressure range over which each set of data was obtained are noted in the figures.

Data presented for angles of attack from 2.0° to 2.5° generally represent straight and level flight. For angles of attack from 2.5° to 3.5°, the data generally represent pullup and climb maneuvers, and for angles of attack greater than 3.5°, the data generally represent measurements taken during turn maneuvers. No attempts were made to differentiate between the measurements taken during steady conditions and the measurements taken at more transient conditions such as rapid changes in pitch or roll angles.

In figure 8 (for the tank-on aircraft configuration), all measured data are presented. In figure 9 (for the tank-off configuration), the data presented include only those measurements obtained when the free-stream dynamic pressure was less than 24 kPa. This limitation was imposed to reduce the effect of wing aeroelasticity on the results for the tank-off configuration. A further discussion of aeroelastic effects is presented in a later section.

The results of the strain-gage bridge measurements of wing structural loads presented in figures 8 and 9 are summarized in figure 10. Figure 10 presents the variation with Mach number of the slope and the intercept of the least-squares straight-line fit to the measured data for both the tank-on and the tank-off aircraft configurations. The data points shown in figure 10 are only for those Mach number conditions where data were available in figures 8 and 9 for an angle-of-attack range equal to or greater than 3°. For bending-moment loads, there is little variation of slope with change in Mach number or aircraft configuration, but there is a large change in the intercept angle with changes in aircraft configuration and changes in Mach number, particularly in the transonic speed range. For shear and torsion loads, there is some variation of slope with Mach number variation but essentially no difference in slope due to configuration changes. There are, however, large changes in intercept which occur because of both Mach number and configuration changes.

Wingloads From Measured Pressure Distributions

In addition to the instrumentation of the left semispan of the test wing (22 strain-gage bridges), instrumentation was installed on the right semispan to measure differential pressure at 29 locations. The results from these pressure measurements are reported in reference 6. For 13 of these test conditions, the chordwise differential pressure distributions, at semispan locations of 0.343, 0.802, and 1.306 m, were integrated to determine the normal (shear) force per unit width at each location. These values of normal force were plotted as a function of semispan location, and a curve was fitted to the data with the additional boundary condition that the normal force must be zero at the semispan tip. The area and the first moment of the area under each curve from the tip to each of the strain-gage bridge stations were then determined. These calculations gave the equivalent shear and bending moment at each strain-gage bridge station. The locations of the chordwise center of pressure, as a function of the semispan location, were also established from the measurements of differential pressures. These locations allowed determination of torque loads. The aerodynamic load from the pressure distribution is essentially the net load because the inertia loads are very small in comparison (that is, the weight of the wing is small in relation to the total weight of the aircraft).

The wingloads, shear (V), bending moment (M), and torque (T), as determined by use of pressure measurements, are shown in figures 8(e), 9(e), and 9(g) as are the loads measured by the calibrated strain-gage bridges. In most instances, there is good agreement between the two types of measurements. Although there was some concern about the adequacy of the strain-gage bridge calibration for the outboard station, the excellent agreement in loads measured by the two methods gives increased confidence in the strain-gage bridge calibration procedures used.

Wingloads From Calculated Pressure Distributions

Theoretical predictions of wing shear, moment, and torque loads as a function of angle of attack for each of the three wing stations were obtained for a limited number of Mach number values by the integration of calculated wing aerodynamic pressure distributions. The pressure distributions were calculated for a rigid structure by using the finite-element analysis method described in reference 8. The aerodynamic paneling scheme used for the analysis is shown in figure 11. The fuselage was represented as a cone cylinder, considered representative of the external-fuel-tank-off aircraft configuration. The analysis method used did not have provisions for properly modeling the external-fuel-tank-on aircraft configuration. The theoretical predictions of wing structural loads are presented in figure 9 (except for the transonic range) as are the measured wing structural loads in order to allow for direct comparisons with the measured values of loads for the tank-off aircraft configuration. For the bending-moment loads, the measured values at the inboard station are greater than the theoretical estimates. For the midwing and the outboard wing stations, the theoretical estimates for bending-moment loads are in close agreement with measured values. In all cases, the measured shear and torque loads are greater than the theoretical estimates.

Aeroelastic Effects on Wingloads

The standard wing for the drone aircraft is a relatively rigid structure because of its design load value (5g), construction method, and low aspect ratio. Even so, aeroelastic effects (structural deformation caused by applied aerodynamic loads) were anticipated. Sufficient data at significantly different dynamic pressure levels were available to evaluate aeroelastic effects at Mach numbers of 1.00 ± 0.025 for the tank-off aircraft configuration. Figure 12 presents the data for loads measurements obtained in this Mach number interval for both low and high levels of dynamic pressure. The lower level includes measurements acquired at dynamic pressures ranging between 13.5 and 18.5 kPa (identical to fig. 9(g)). The higher level includes measurements acquired at dynamic pressures ranging between 28.9 and 39.6 kPa. There is a more than a two to one difference in the midpoint dynamic pressure for the two ranges.

As indicated by figure 12, the largest aeroelastic effect occurs at the outboard wing station where there is a large change in the slopes for the load measurements. At the midwing station there is also a significant change in slope for the loads measurements. At the inboard station the torque load measurements still indicate a change in slope, whereas for shear and moment loads the primary difference between measurements obtained at low and high levels of dynamic pressure is in the intercept value and not in the slope changes.

Although some measurements were available at the high dynamic pressure level for other Mach numbers, there was insufficient data to establish trends. As mentioned earlier, the data presented in figure 9 were limited to values obtained at dynamic pressures of less than 24 kPa.

Comparison With Previous Measurements

Flight loads measurements obtained from calibrated strain-gage bridges were previously obtained on an identical wing for a single wing station with the reference axis system oriented parallel and perpendicular to the wing 40-percent chord line as reported in reference 5. The differences in axis system orientation and the noncoincidence of wing stations between the wing of reference 5 and that of the present report preclude an accurate direct comparison of measured loads. However, an indirect comparison of the measured loads can be obtained by considering the respective agreements between measured and calculated loads for the two sets of data. Although different numbers and arrangements of panels were used for the respective calculations, the calculated load distributions were essentially the same.

The data from reference 5 indicate close agreement between measured and calculated values of shear, bending moment, and torque loads for the tank-off configuration at a Mach number of 0.8 (subsonic) and a Mach number of 1.2 (supersonic). The data presented in this report show fair to good agreement between measured and calculated values for a Mach number of 1.2 (fig. 9(k)). For a Mach number of 0.8 (fig. 9(c)) and for all subsonic speeds for which data were obtained, the measured data for angles of attack from 1^{o} to 3^{o} are generally in close agreement with calculated values; however, the data points obtained at higher angles of attack indicate substantially higher loads than calculated, particularly at the inboard station. The differences in slope between the measured and calculated loads are approximately 30 percent at the inboard station. Thus, the measured values of loads as presented in this report for subsonic conditions may be assumed to be higher than those of reference 5.

Although the evidence is not conclusive, some of the differences between the results of reference 5 and the results in this report may be caused by aeroelastic effects. It is noted that the test dynamic pressure range was relatively low and similar for the flights of both wings at a Mach number of 1.2, whereas the dynamic pressures at a Mach number of 0.8 for the reference 5 test conditions were approximately twice those for the data presented in this report.

CONCLUDING REMARKS

A low-aspect-ratio, thin, swept wing with a structural skin, full-depth honeycomb core construction was instrumented with strain-gage bridges mounted externally on the wing surface at three spanwise stations. The wing calibration procedure consisted of applying calibration loadings to the wing and measuring the electrical imbalance, or output, of the strain-gage bridges. Linear regression analysis techniques were then used to derive load coefficients for equations which gave the applied wing loadings as a function of the output of selected strain-gage bridges. Flight-test measurements of strain-gage bridge outputs were then used to compute the measured wing structural loads. Evaluation of the calibration procedure and comparison of the test results with pressure measurements and theoretical calculations indicate the following:

1. The statistical evaluation of errors provided by the regression analysis was useful in determining which strain-gage bridge outputs should be used for load equations.

2. The use of more than three strain-gage bridges in any load equation generally resulted in large errors associated with one or more of the load coefficients.

3. Evaluation of all possible combinations of one, two, or three strain-gage bridges for load equations allowed selection based on accuracy of both the probable error criteria and the measured range of accuracy.

4. The measured range of accuracy for the selected load equations, as determined by their capability to estimate multipoint calibration loadings, varied from ±3 percent for bending-moment loads at the inboard station to ±14 percent for torque loads at the midwing station.

5. The slope of the linear relationship between structural load and angle of attack was essentially the same for both aircraft configurations (that is, external fuel tank on or external fuel tank off).

6. For each wing station, the slope of the linear relationship between structural load and angle of attack changed very little for bending-moment loads over the Mach number range tested, but there were small changes in slope with Mach number for shear and torsion loads.

7. There are significant differences in the angle of attack at zero wing loading (shear, bending moment, and torsion) between aircraft configurations and also for variations in Mach number in the transonic speed range.

8. Flight loads as determined from measurements of differential pressure on the opposite wing semispan were in reasonable agreement with those determined from the strain-gage bridge measurements.

9. Theoretical estimates of wingloads from an aerodynamic finite-element analysis method were lower than the measured values in most cases.

10. Measured aeroelastic effects indicated a trend to lower structural load ratios at higher dynamic pressures, a trend which is in agreement with theoretical analysis.

Langley Research Center
National Aeronautics and Space Administration
Hampton, VA 23665
November 22, 1976

REFERENCES

1. Skopinski, T. H.; Aiken, William S., Jr.; and Huston, Wilber B.: Calibration of Strain-Gage Installations in Aircraft Structures for the Measurement of Flight Loads. NACA Rep. 1178, 1954. (Supersedes NACA TN 2993.)

2. Hovell, P. B.; Webber, D. A.; and Roberts, T. A.: The Interpretation of Strain Measurements for Flight Load Determination. C.P. No. 839, Brit. A.R.C., Aug. 1964.

3. Hovell, P. B.; Webber, D. A.; and Roberts, T. A.: The Use of Calibrated Strain Gauges for Flight Load Determination. C.P. No. 1041, Brit. A.R.C., July 1968.

4. Sefic, Walter J.; and Reardon, Lawrence F.: Loads Calibration of the Airplane. NASA YF-12 Flight Loads Program, NASA TM X-3061, 1974, pp. 61-107.

5. Peele, Ellwood L.; and Eckstrom, Clinton V.: Strain-Gage Bridge Calibration and Flight Loads Measurements on a Low-Aspect-Ratio Thin Wing. NASA TN D-7979, 1975.

6. Byrdsong, Thomas A.: Flight Measurements of Lifting Pressures for a Thin Low-Aspect-Ratio Wing at Subsonic, Transonic, and Low Supersonic Speeds. NASA TM X-3405, 1977.

7. Eckstrom, Clinton V.; and Peele, Ellwood L.: Flight Assessment of a Large Supersonic Drone Aircraft for Research Use. NASA TM X-3259, 1975.

8. Carmichael, Ralph L.; Castellano, Charles R.; and Chen, Chuan F.: The Use of Finite Element Methods for Predicting the Aerodynamics of Wing-Body Combinations. Analytical Methods in Aircraft Aerodynamics, NASA SP-228, 1970, pp. 37-51.

TABLE I. - CALIBRATION WING LOADINGS AND STRAIN-GAGE BRIDGE OUTPUTS FOR INBOARD STATION

Load point	Calibration load, N	Wing loading			Strain-gage bridge output, mV, for –									
		Shear, N	Bending moment, N-m	Torque, N-m	μ_{1B}	μ_{2B}	μ_{3B}	μ_{4B}	μ_{5B}	μ_{1T}	μ_{2T}	μ_{3T}	μ_{4T}	μ_{5T}
1	1246	1246	237	141	0.270	0.294	0.277	0.061	0.012	-0.105	-0.015	-0.012	-0.036	-0.002
2	1246	1246	237	387	.222	.267	.309	.041	.001	-.143	-.213	-.164	-.090	-.013
3	1246	1246	237	632	.180	.230	.262	-.006	-.037	-.171	-.303	-.410	-.184	-.030
4	1246	1246	237	897	.142	.202	.200	-.096	-.099	-.205	-.406	-.597	-.429	-.077
5	1246	1246	237	1124	.106	.167	.159	-.207	-.153	-.243	-.516	-.813	-.612	-.370
6	890	890	452	435	.293	.438	.608	.215	.078	-.236	-.381	-.416	-.310	-.075
7	890	890	452	570	.266	.406	.585	.203	.086	-.255	-.450	-.562	-.443	-.136
8	890	890	452	705	.240	.376	.551	.178	.097	-.274	-.513	-.699	-.583	-.215
9	890	890	452	840	.214	.348	.521	.147	.107	-.290	-.574	-.830	-.720	-.307
10	890	890	452	975	.189	.321	.488	.116	.114	-.311	-.642	-.964	-.858	-.402
11	445	445	339	351	.179	.286	.447	.196	.107	-.179	-.324	-.416	-.366	-.125
12	445	445	339	402	.166	.275	.430	.184	.110	-.185	-.346	-.467	-.418	-.159
13	445	445	339	454	.158	.268	.421	.175	.115	-.193	-.371	-.518	-.472	-.192
14	445	445	339	505	.149	.254	.409	.164	.121	-.201	-.396	-.572	-.526	-.227
15	445	445	339	556	.138	.242	.397	.153	.124	-.208	-.419	-.620	-.575	-.258

TABLE II.- CALIBRATION WING LOADINGS AND STRAIN-GAGE BRIDGE OUTPUTS FOR MIDWING STATION

Load point	Calibration load, N	Wind loading			Strain-gage bridge output, mV, for –					
		Shear, N	Bending moment, N-m	Torque, N-m	μ_{6B}	μ_{7B}	μ_{8B}	μ_{6T}	μ_{7T}	μ_{8T}
1	1246	0	0	0	-0.003	0.001	0.003	0.001	0.006	0.002
2	1246	0	0	0	.034	-.009	-.008	-.019	-.013	-.003
3	1246	0	0	0	.018	-.029	-.030	-.062	-.049	-.008
4	1246	0	0	0	-.018	-.090	-.046	-.155	.009	-.004
5	1246	0	0	0	-.113	-.264	.130	-.278	.024	.303
6	890	890	113	435	.386	.159	.036	-.159	-.034	-.009
7	890	890	113	570	.282	.161	.011	-.364	-.183	-.048
8	890	890	113	705	.227	.135	-.067	-.453	-.374	-.114
9	890	890	113	840	.162	.048	-.137	-.556	-.256	-.294
10	890	890	113	975	.088	-.024	-.308	-.662	-.796	-.608
11	445	445	170	351	.296	.378	.181	-.365	-.330	-.128
12	445	445	170	402	.255	.343	.181	-.404	-.429	-.209
13	445	445	170	454	.226	.318	.194	-.446	-.528	-.309
14	445	445	170	505	.192	.287	.192	-.488	-.622	-.419
15	445	445	170	556	.159	.254	.185	-.526	-.708	-.522

TABLE III.- CALIBRATION WING LOADINGS AND STRAIN-GAGE BRIDGE OUTPUTS FOR OUTBOARD STATION

Load point	Calibration load, N	Wing loading			Strain-gage bridge output, mV, for –					
		Shear, N	Bending moment, N-m	Torque, N-m	μ_{9B}	μ_{10B}	μ_{11B}	μ_{9T}	μ_{10T}	μ_{11T}
1	1246	0	0	0	0.000	0.000	-0.000	-0.001	0.000	0.000
2	1246	0	0	0	.002	-.001	-.002	-.002	.001	.000
3	1246	0	0	0	.006	-.002	-.003	-.003	-.005	.000
4	1246	0	0	0	-.007	-.002	.000	-.003	.003	.000
5	1246	0	0	0	-.071	-.002	.050	-.017	.060	.026
6	890	0	0	0	.000	-.001	-.002	.003	.003	.001
7	890	0	0	0	.062	-.017	-.010	-.038	-.016	.000
8	890	0	0	0	.039	-.047	-.050	-.095	-.092	-.020
9	890	0	0	0	.006	-.113	-.100	-.145	-.006	-.040
10	890	0	0	0	-.104	-.306	.080	-.389	-.037	.394
11	445	445	56.5	351	.370	.188	.046	-.166	-.070	-.018
12	445	445	56.5	402	.265	.179	.022	-.299	-.203	-.063
13	445	445	56.5	454	.229	.170	-.019	-.382	-.397	-.127
14	445	445	56.5	505	.175	.094	-.055	-.475	-.528	-.321
15	445	445	56.5	556	.120	.033	-.176	-.559	-.656	-.564

TABLE IV.- INBOARD STATION WING LOADINGS AND STRAIN-GAGE BRIDGE OUTPUTS

FOR MULTIPOINT LOADING CALIBRATION SET A

Loading step	Incremental applied load, N	Location	Wing loading			Strain-gage bridge output, mV, for –									
			Shear, N	Bending moment, N-m	Torque, N-m	μ_{1B}	μ_{2B}	μ_{3B}	μ_{4B}	μ_{5B}	μ_{1T}	μ_{2T}	μ_{3T}	μ_{4T}	μ_{5T}
1	667	1	667	127	76	0.147	0.158	0.145	0.034	0.005	-0.050	0.004	-0.002	-0.019	-0.001
2	667	3	1335	254	414	.244	.283	.284	.029	-.016	-.142	-.155	-.223	-.117	-.017
3	444	6	1779	480	631	.396	.512	.592	.133	.022	-.259	-.347	-.433	-.277	-.062
4	444	8	2224	706	984	.515	.704	.863	.222	.071	-.394	-.597	-.787	-.565	-.168
5	222	11	2446	876	1160	.607	.850	1.082	.315	.125	-.487	-.760	-1.004	-.744	-.230
6	667	1	3114	1003	1236	.774	1.019	1.239	.348	.133	-.542	-.748	-1.008	-.761	-.231
7	667	3	3781	1130	1574	.881	1.149	1.386	.346	.115	-.638	-.913	-1.238	-.857	-.245
8	444	6	4226	1356	1791	1.045	1.376	1.704	.459	.159	-.765	-1.105	-1.453	-1.011	-.281
9	444	8	4671	1582	2144	1.176	1.566	1.981	.547	.213	-.907	-1.362	-1.809	-1.293	-.384
10	222	11	4893	1751	2320	1.272	1.714	2.209	.646	.270	-1.000	-1.526	-2.024	-1.474	-.445
11	-667	1	4226	1624	2244	1.118	1.543	2.049	.606	.261	-.951	-1.540	-2.029	-1.456	-.443
12	-667	3	3559	1497	1906	1.024	1.414	1.893	.603	.272	-.864	-1.386	-1.809	-1.362	-.432
13	-444	6	3114	1271	1689	.877	1.185	1.570	.486	.228	-.749	-1.204	-1.600	-1.209	-.395
14	-444	8	2670	1045	1336	.761	.994	1.285	.394	.176	-.618	-.958	-1.252	-.923	-.292
15	-222	11	2447	875	1160	.669	.848	1.059	.297	.120	-.525	-.797	-1.039	-.742	-.231
16	-667	1	1779	749	1084	.521	.690	.907	.265	.112	-.474	-.806	-1.040	-.726	-.230
17	-667	3	1112	621	746	.423	.563	.766	.270	.132	-.380	-.645	-.814	-.629	-.215
18	-444	6	667	395	529	.273	.340	.460	.166	.093	-.256	-.457	-.599	-.477	-.176
19	-444	8	222	169	176	.134	.151	.200	.087	.048	-.105	-.190	-.229	-.190	-.067
20	-222	11	0	0	0	.019	.006	-.008	-.004	-.004	.003	-.011	-.009	-.009	-.004

TABLE V.- MIDWING STATION WING LOADINGS AND STRAIN-GAGE BRIDGE OUTPUTS FOR MULTIPOINT LOADING CALIBRATION SET A

Loading step	Incremental applied load, N	Location	Wing loading			Strain-gage bridge output, mV, for –					
			Shear, N	Bending moment, N-m	Torque, N-m	μ_{6B}	μ_{7B}	μ_{8B}	μ_{6T}	μ_{7T}	μ_{8T}
1	667	1	0	0	0	-0.002	0.001	0.002	0.001	0.002	0.001
2	667	3	0	0	0	.008	-.014	-.015	-.030	-.023	-.004
3	444	6	445	56.5	217.5	.205	.065	.005	-.108	-.035	-.004
4	444	8	889	112.9	570.0	.319	.128	-.030	-.331	-.249	-.058
5	222	11	1112	197.5	745.6	.466	.315	.058	-.514	-.414	-.124
6	667	1	1112	197.5	745.6	.464	.318	.061	-.511	-.409	-.124
7	667	3	1112	197.5	745.6	.475	.302	.045	-.544	-.438	-.130
8	444	6	1557	254.0	963.1	.695	.393	.068	-.620	-.451	-.135
9	444	8	2001	310.5	1315.5	.815	.467	.039	-.848	-.669	-.190
10	222	11	2224	395.1	1491.1	.967	.662	.135	-1.037	-.842	-.258
11	-667	1	2224	395.1	1491.1	.967	.658	.131	-1.043	-.848	-.260
12	-667	3	2224	395.1	1491.1	.956	.673	.146	-1.009	-.818	-.255
13	-444	6	1779	338.6	1273.6	.736	.580	.121	-.932	-.803	-.252
14	-444	8	1335	282.1	921.2	.619	.510	.152	-.706	-.586	-.196
15	-222	11	1112	197.5	745.6	.469	.316	.059	-.520	-.415	-.130
16	-667	1	1112	197.5	745.6	.469	.314	.056	-.522	-.419	-.131
17	-667	3	1112	197.5	745.6	.460	.330	.074	-.488	-.391	-.126
18	-444	6	667	141.0	528.0	.259	.247	.053	-.413	-.377	-.123
19	-444	8	222	84.5	175.6	.147	.187	.089	-.186	-.162	-.068
20	-222	11	0	0	0	.001	0	.001	-.001	.004	-.003

TABLE VI. - OUTBOARD STATION WING LOADINGS AND STRAIN-GAGE BRIDGE OUTPUTS FOR MULTIPOINT LOADING CALIBRATION SET A

Loading step	Incremental applied load, N	Location	Wing loading			Strain-gage bridge output, mV, for –					
			Shear, N	Bending moment, N-m	Torque, N-m	μ_{9B}	μ_{10B}	μ_{11B}	μ_{9T}	μ_{10T}	μ_{11T}
1	667	1	0	0	0	0	0.001	0	0	0	0.001
2	667	3	0	0	0	.003	0	-.002	-.002	-.003	0
3	444	6	0	0	0	.003	.001	-.002	.005	.003	.004
4	444	8	0	0	0	.023	-.021	-.027	-.040	-.039	-.004
5	222	11	222	84.6	175.6	.203	.071	-.005	-.128	-.075	-.012
6	667	1	222	84.6	175.6	.202	.071	-.005	-.129	-.075	-.012
7	667	3	222	84.6	175.6	.206	.071	-.007	-.132	-.072	-.013
8	444	6	222	84.6	175.6	.205	.072	-.005	-.126	-.075	-.011
9	444	8	222	84.6	175.6	.226	.049	-.031	-.172	-.121	-.022
10	222	11	445	169.2	351.2	.419	.152	-.005	-.264	-.161	-.033
11	-667	1	445	169.2	351.2	.419	.151	-.006	-.266	-.162	-.034
12	-667	3	445	169.2	351.2	.415	.152	-.005	-.264	-.158	-.033
13	-444	6	445	169.2	351.2	.416	.149	-.006	-.269	-.162	-.032
14	-444	8	445	169.2	351.2	.395	.173	.019	-.223	-.114	-.022
15	-222	11	222	84.6	175.6	.204	.072	-.006	-.132	-.074	-.012
16	-667	1	222	84.6	175.6	.204	.070	-.007	-.132	-.076	-.012
17	-667	3	222	84.6	175.6	.201	.072	-.004	-.130	-.071	-.011
18	-444	6	222	84.6	175.6	.201	.071	-.006	-.133	-.075	-.011
19	-444	8	222	84.6	175.6	.181	.093	.020	-.087	-.031	-.003
20	-222	11	0	0	0	.001	.001	-.002	.001	-.005	.007

TABLE VII.- INBOARD STATION WING LOADINGS AND STRAIN-GAGE BRIDGE OUTPUTS

FOR MULTIPOINT LOADING CALIBRATION SET B

Loading step	Incremental applied load, N	Location	Wing loading			Strain-gage bridge output, mV, for –									
			Shear, N	Bending moment, N-m	Torque, N-m	μ_{1B}	μ_{2B}	μ_{3B}	μ_{4B}	μ_{5B}	μ_{1T}	μ_{2T}	μ_{3T}	μ_{4T}	μ_{5T}
1	667	2	667	127	207	0.115	0.142	0.164	0.022	-0.001	-0.075	-0.112	-0.086	-0.047	-0.006
2	667	4	1335	254	678	.194	.248	.266	-.036	-.055	-.186	-.327	-.404	-.277	-.041
3	444	6	1779	480	895	.339	.465	.570	.070	-.017	-.303	-.518	-.615	-.437	-.075
4	444	10	2224	706	1383	.450	.624	.803	.123	.040	-.469	-.851	-1.106	-.861	-.271
5	222	12	2446	876	1584	.555	.762	1.004	.206	.097	-.578	-1.034	-1.352	-1.063	-.343
6	667	2	3114	1003	1791	.689	.920	1.180	.232	.099	-.665	-1.150	-1.445	-1.117	-.348
7	667	4	3781	1130	2262	.782	1.032	1.278	.172	.054	-.795	-1.377	-1.783	-1.337	-.381
8	444	6	4226	1356	2479	.945	1.256	1.581	.279	.097	-.927	-1.571	-2.000	-1.488	-.418
9	444	10	4671	1582	2967	1.048	1.419	1.819	.329	.164	-1.077	-1.902	-2.500	-1.899	-.609
10	222	12	4893	1751	3168	1.136	1.557	2.028	.413	.223	-1.179	-2.083	-2.742	-2.098	-.682
11	-667	2	4226	1624	2960	1.023	1.398	1.839	.379	.216	-1.107	-1.979	-2.655	-2.049	-.676
12	-667	4	3559	1497	2490	.953	1.289	1.720	.426	.256	-1.001	-1.770	-2.331	-1.826	-.643
13	-444	6	3114	1271	2273	.809	1.065	1.406	.314	.213	-.887	-1.587	-2.120	-1.673	-.607
14	-444	10	2670	1045	1785	.720	.905	1.157	.256	.145	-.735	-1.274	-1.635	-1.256	-.416
15	-222	12	2447	875	1584	.637	.769	.943	.168	.088	-.643	-1.105	-1.401	-1.053	-.341
16	-667	2	1779	749	1377	.519	.624	.776	.148	.087	-.567	-.992	-1.312	-1.007	-.336
17	-667	4	1112	621	906	.443	.517	.671	.206	.138	-.454	-.778	-.990	-.784	-.303
18	-444	6	667	395	689	.294	.295	.373	.104	.101	-.331	-.588	-.771	-.633	-.265
19	-444	10	222	169	201	.180	.131	.145	.058	.046	-.159	-.255	-.264	-.212	-.066
20	-222	12	0	0	0	.071	-.008	-.050	-.023	-.007	-.047	-.061	-.010	-.006	.012

TABLE VIII.- MIDWING STATION WING LOADINGS AND STRAIN-GAGE BRIDGE OUTPUTS FOR MULTIPOINT LOADING CALIBRATION SET B

Loading step	Incremental applied load, N	Location	Wing loading			Strain-gage bridge output, mV, for –					
			Shear, N	Bending moment, N-m	Torque, N-m	μ_{6B}	μ_{7B}	μ_{8B}	μ_{6T}	μ_{7T}	μ_{8T}
1	667	2	0	0	0	0.018	-0.005	-0.004	-0.012	-0.007	0
2	667	4	0	0	0	.008	-.052	-.028	-.092	-.001	-.004
3	444	6	445	56.5	217.5	.196	.024	-.010	-.173	-.018	-.010
4	444	10	889	112.9	705.0	.240	.011	-.166	-.504	-.412	-.309
5	222	12	1112	197.5	906.3	.368	.182	-.075	-.706	-.279	-.414
6	667	2	1112	197.5	906.3	.386	.177	-.078	-.720	-.636	-.418
7	667	4	1112	197.5	906.3	.377	.128	-.103	-.806	-.632	-.424
8	444	6	1557	254.0	1123.8	.582	.212	-.083	-.889	-.648	-.431
9	444	10	2001	310.5	1611.3	.627	.201	-.233	-1.227	-1.051	-.738
10	222	12	2224	395.1	1812.5	.754	.371	-.142	-1.430	-1.266	-.845
11	-667	2	2224	395.1	1812.5	.736	.375	-.140	-1.415	-1.260	-.845
12	-667	4	2224	395.1	1812.5	.746	.425	-.115	-1.328	-1.265	-.838
13	-444	6	1779	338.6	1595.0	.540	.338	-.137	-1.246	-1.250	-.833
14	-444	10	1335	282.1	1107.5	.497	.349	.013	-.912	-.847	-.524
15	-222	12	1112	197.5	906.3	.371	.181	-.075	-.712	-.634	-.421
16	-667	2	1112	197.5	906.3	.352	.186	-.072	-.699	-.627	-.420
17	-667	4	1112	197.5	906.3	.362	.232	-.048	-.618	-.633	-.415
18	-444	6	667	141.0	688.7	.173	.155	-.066	-.536	-.616	-.410
19	-444	10	222	84.5	201.3	.128	.168	.089	-.204	-.220	-.110
20	-222	12	0	0	0	.001	-.003	0	-.002	-.004	-.006

TABLE IX.- OUTBOARD STATION WING LOADINGS AND STRAIN-GAGE BRIDGE OUTPUTS

FOR MULTIPOINT LOADING CALIBRATION SET B

Loading step	Incremental applied load, N	Location	Wing loading			Strain-gage bridge output, mV, for –					
			Shear, N	Bending moment, N-m	Torque, N-m	μ_{9B}	μ_{10B}	μ_{11B}	μ_{9T}	μ_{10T}	μ_{11T}
1	667	2	0	0	0	0.001	-0.002	-0.001	-0.002	-0.001	0
2	667	4	0	0	0	-.004	-.001	-.001	-.004	-.001	-.002
3	444	6	0	0	0	-.004	0	-.001	-.003	.001	-.002
4	444	10	0	0	0	-.054	-.150	.036	-.194	-.017	.190
5	222	12	222	84.6	201.3	.077	-.062	.047	-.344	-.122	.156
6	667	2	222	84.6	201.3	.077	-.063	.045	-.347	-.126	.154
7	667	4	222	84.6	201.3	.073	-.063	.045	-.349	-.126	.153
8	444	6	222	84.6	201.3	.073	-.062	.046	-.346	-.123	.154
9	444	10	222	84.6	201.3	.073	-.219	.084	-.547	-.148	.373
10	222	12	445	169.2	402.6	.020	-.136	.092	-.695	-.249	.345
11	-667	2	445	169.2	402.6	.148	-.136	.093	-.694	-.248	.344
12	-667	4	445	169.2	402.6	.147	-.136	.094	-.691	-.248	.345
13	-444	6	445	169.2	402.6	.152	-.138	.094	-.694	-.251	.343
14	-444	10	445	169.2	402.6	.205	.019	.056	-.494	-.226	.124
15	-222	12	222	84.6	201.3	.078	-.063	.047	-.347	-.126	.153
16	-667	2	222	84.6	201.3	.077	-.062	.048	-.345	-.126	.152
17	-667	4	222	84.6	201.3	.081	-.063	.049	-.343	-.127	.152
18	-444	6	222	84.6	201.3	.080	-.063	.049	-.345	-.129	.151
19	-444	10	222	84.6	201.3	.131	.087	.009	-.152	-.112	-.041
20	-222	12	0	0	0	-.001	-.001	-.001	-.003	-.009	-.009

TABLE X.- SUMMARY OF CAPABILITY OF LOAD EQUATIONS (BASED ON POINT LOAD CALIBRATION DATA) TO ESTIMATE 20 MULTIPOINT LOADING CONDITIONS

(a) Inboard station: (175 possible combinations using 1, 2, or 3 of 10 strain-gage bridges)

Range of ratios of estimated to actual load	Number of combinations capable of estimating loads in each range		
	Shear load	Bending-moment load	Torsion load
0.95 to 1.05	0	29	1
0.90 to 1.10	9	70	13
0.80 to 1.20	43	116	75
0.70 to 1.30	89	154	121
<0.70 or >1.30	86	21	54

(b) Midwing station: (41 possible combinations using 1, 2, or 3 of 6 strain-gage bridges)

Range of ratios of estimated to actual load	Number of combinations capable of estimating loads in each range		
	Shear load	Bending-moment load	Torsion load
0.95 to 1.05	0	1	0
0.90 to 1.10	3	2	0
0.80 to 1.20	8	12	11
0.70 to 1.30	12	17	19
<0.70 to >1.30	29	24	22

(c) Outboard station: (14 possible combinations using 1 or 2 of 4 strain-gage bridges)

Range of ratios of estimated to actual load	Number of combinations capable of estimating loads in each range		
	Shear load	Bending-moment load	Torsion load
0.95 to 1.05	0	0	0
0.90 to 1.10	0	0	2
0.80 to 1.20	1	1	3
0.70 to 1.30	3	3	3
<0.70 or >1.30	11	11	11

TABLE XI. - SUMMARY OF SELECTED STRAIN-GAGE BRIDGES, LOAD COEFFICIENTS, PROBABLE ERRORS, AND ACCURACY EVALUATION FOR WING STATIONS

Load measurement	Selected bridges	Load coefficient ± probable error	Average wing calibration loading	Probable error of load estimate	Measured range of accuracy, percent (a)
Inboard station					
V	2B	4894 ± 218	860 N	±85 N	±10
	4B	-4129 ± 236			
	3T	292 ± 88			
M	2B	528 ± 16	343 N-m	±2.5 N-m	±3
	3B	277 ± 12			
	4T	-174 ± 3			
T	3B	388 ± 62	598 N-m	±33 N-m	±5
	5B	-1947 ± 136			
	3T	-998 ± 36			
Midwing station					
V	6B	1445 ± 258	667 N	±130 N	±10
	6T	-1215 ± 253			
	7T	483 ± 225			
M	6B	89 ± 22	142 N-m	±7 N-m	±6
	7B	218 ± 17			
	6T	-173 ± 7			
T	6B	519 ± 196	579 N-m	±99 N-m	±14
	6T	-1028 ± 102			
Outboard station					
V	10B	1276 ± 63	44.5 N	±23 N	±13
	9T	-935 ± 59			
	10T	220 ± 66			
M	10B	162 ± 8	56.5 N-m	±3 N-m	±13
	9T	-118 ± 7			
	10T	28 ± 8			
T	10B	968 ± 51	454 N-m	±19 N-m	±7
	9T	-684 ± 48			
	10T	-171 ± 54			

[a] Accuracy of load equations in estimating multipoint loading conditions 6 to 15 of both sets A and B.

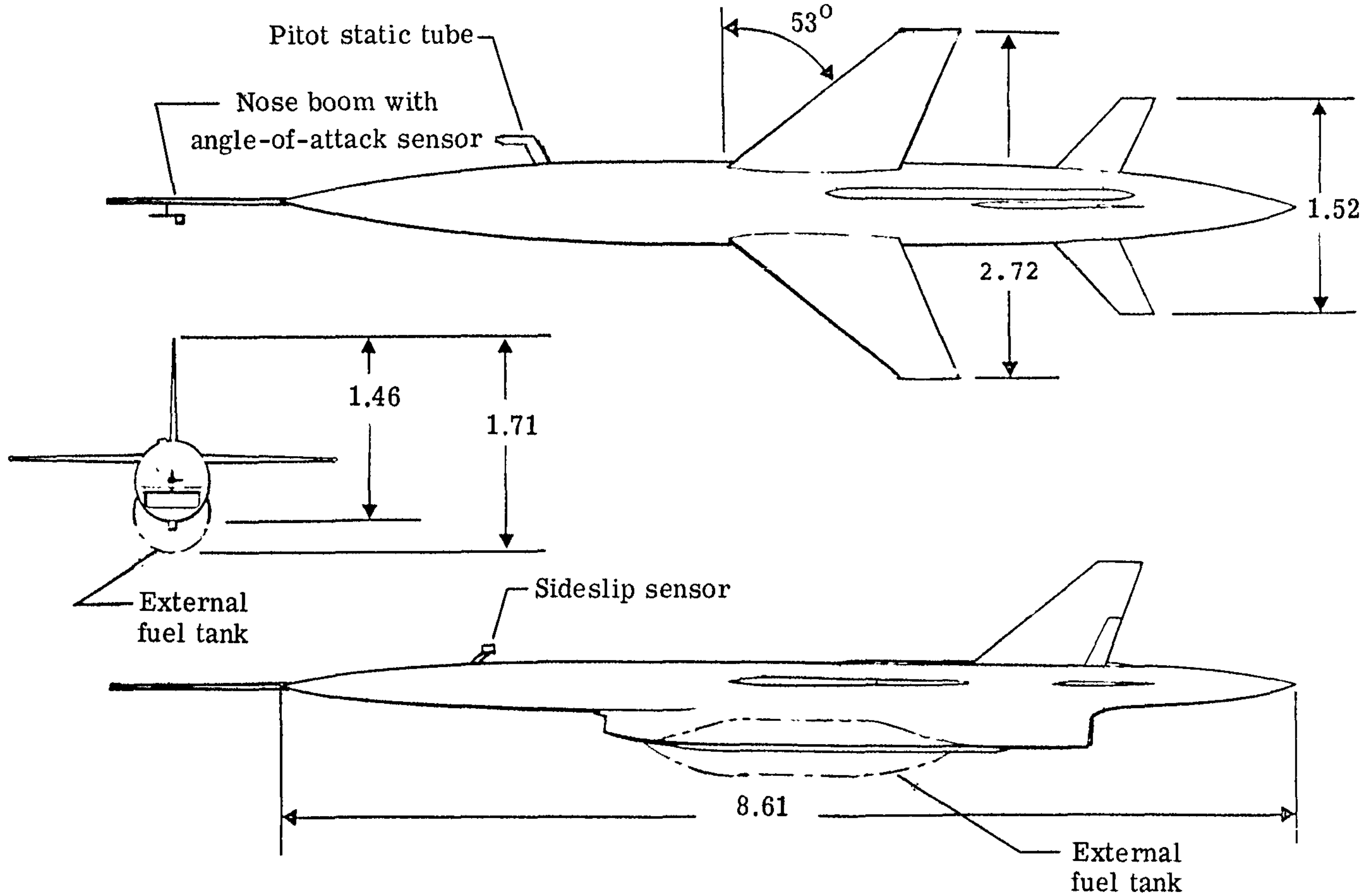

Figure 1.- Three views of test vehicle. Dimensions are in meters.

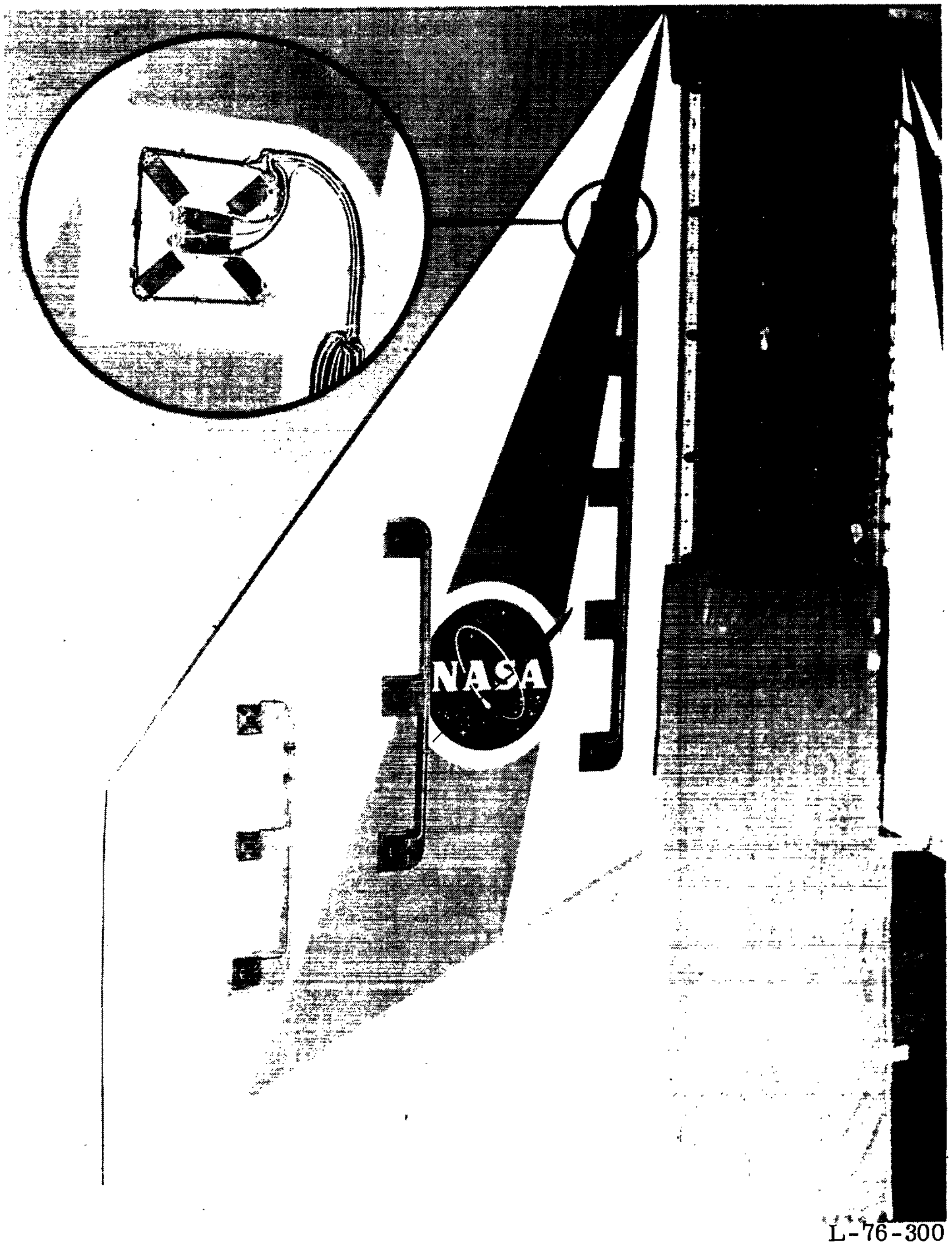

L-76-300

Figure 2.- Upper surface of test wing before strain-gage bridge protective coatings were applied. (Wing tip section removed.)

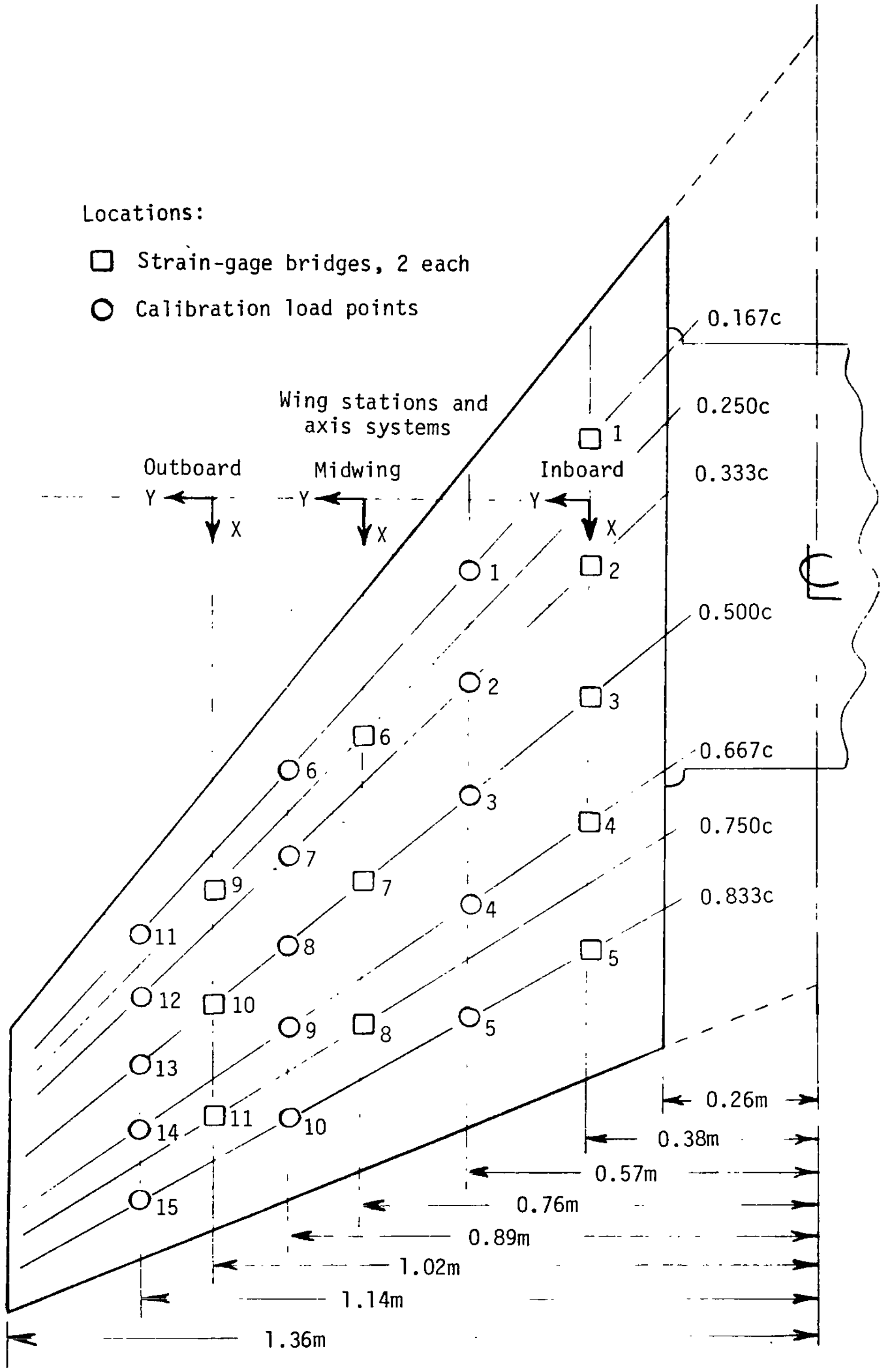

Figure 3.- Calibration load point and strain-gage bridge locations.

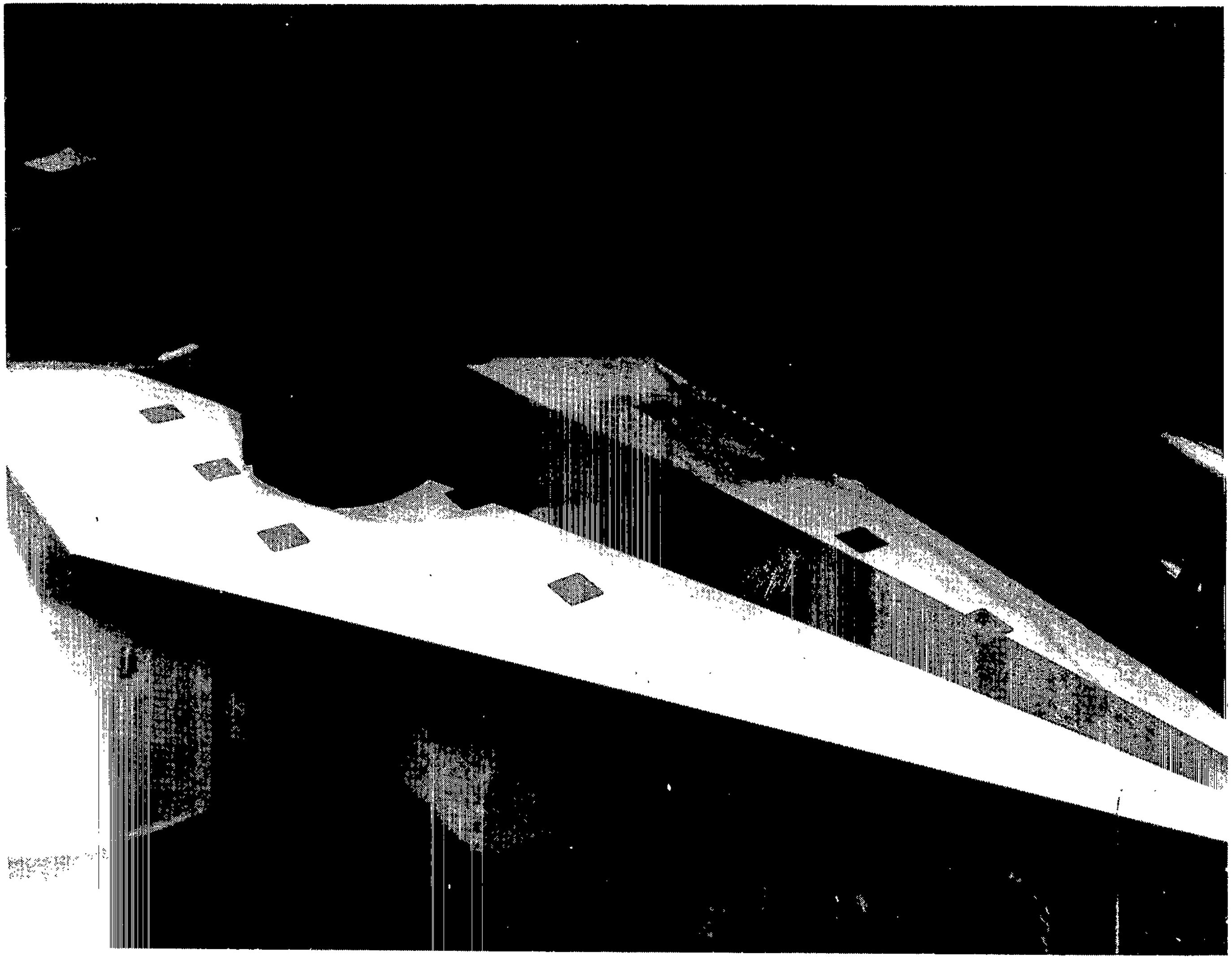

L-73-7022

Figure 4.- Single-point calibration loading with aircraft in inverted position.

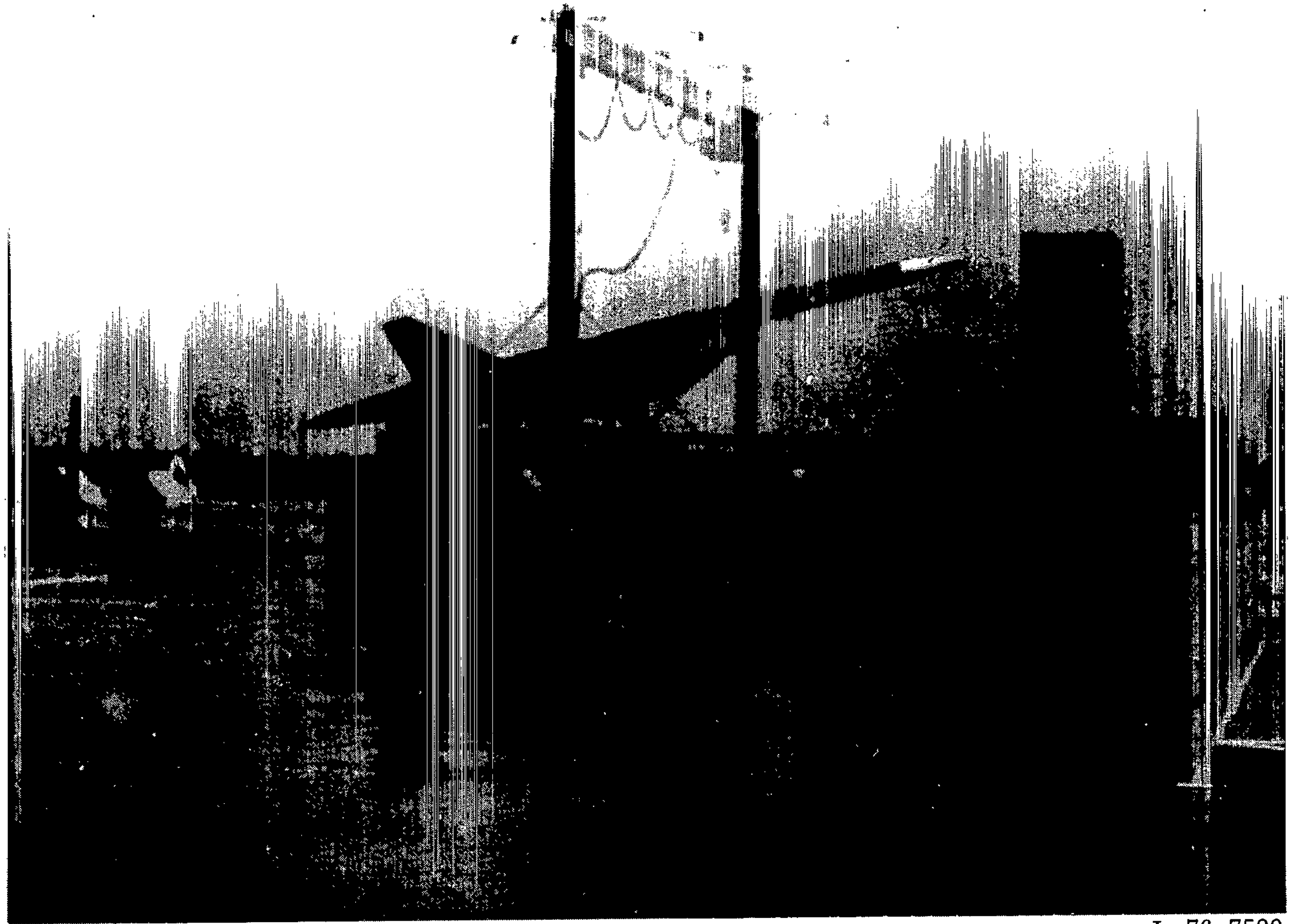

L-76-7500

Figure 5.- Arrangement for rocket-assisted ground launch of drone aircraft.

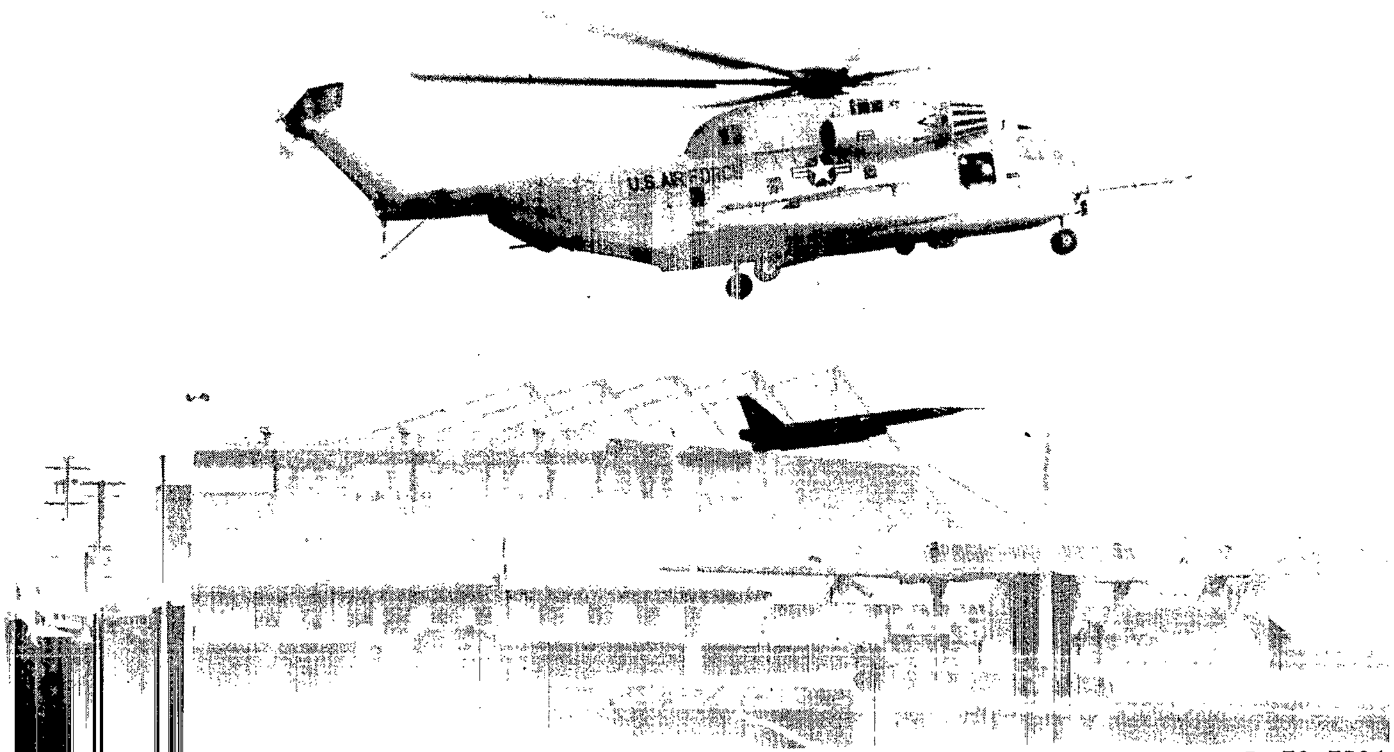

L-76-7501

Figure 6.- Drone aircraft suspended beneath helicopter used for mid-air retrieval system (MARS) recovery.

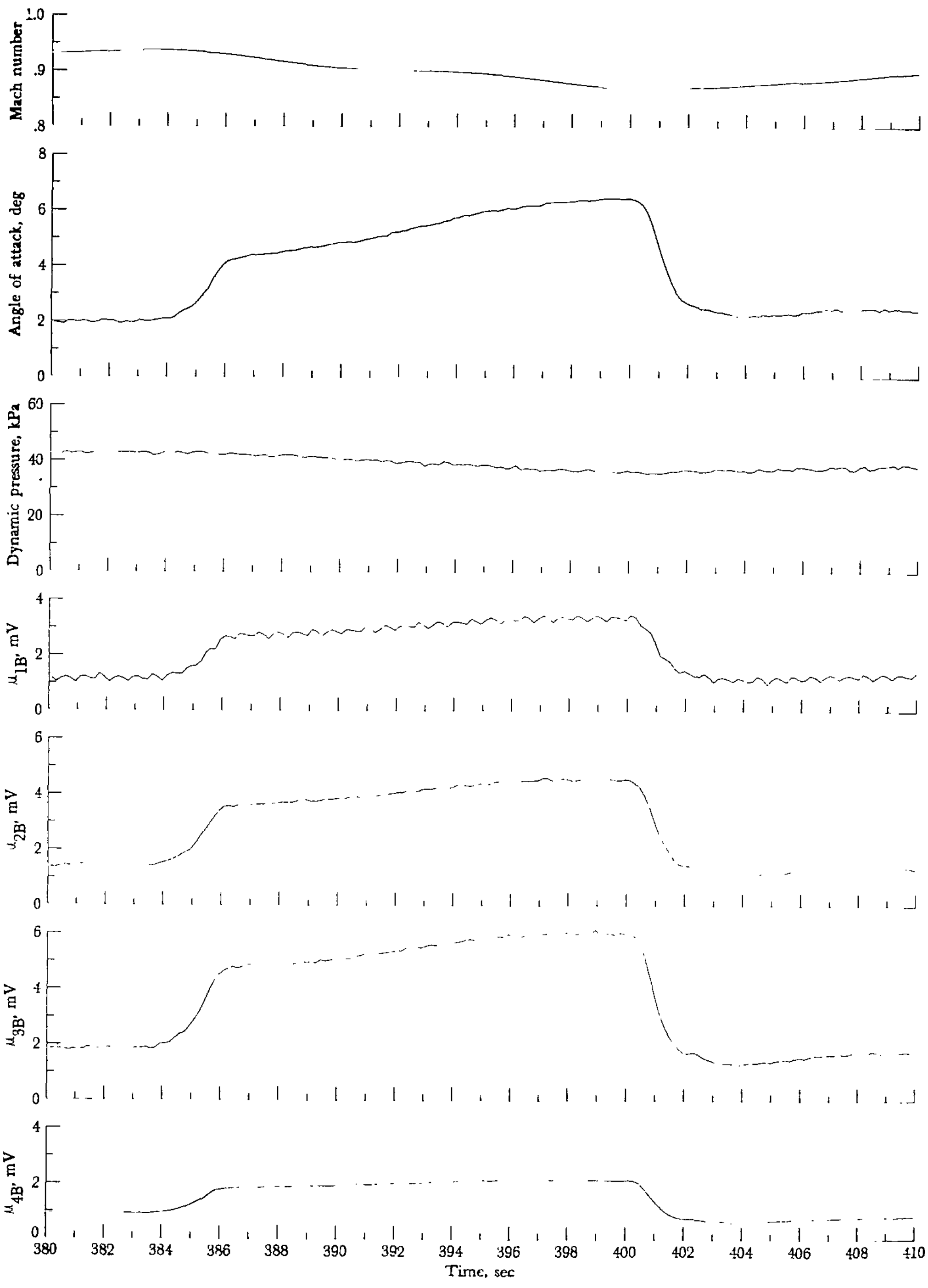

Figure 7.- Sample record of flight measurements (external-fuel-tank-on aircraft configuration).

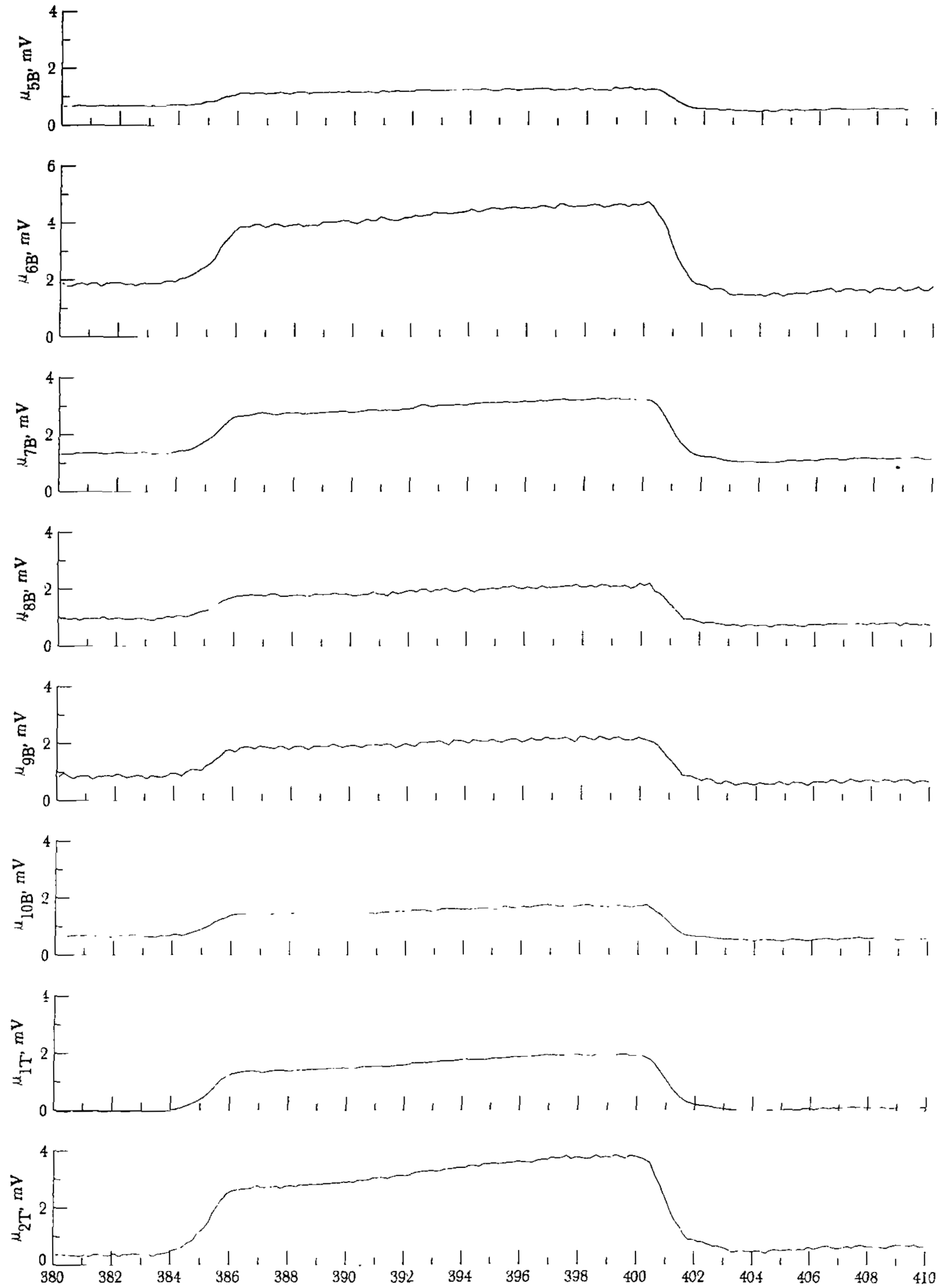

Figure 7.- Continued.

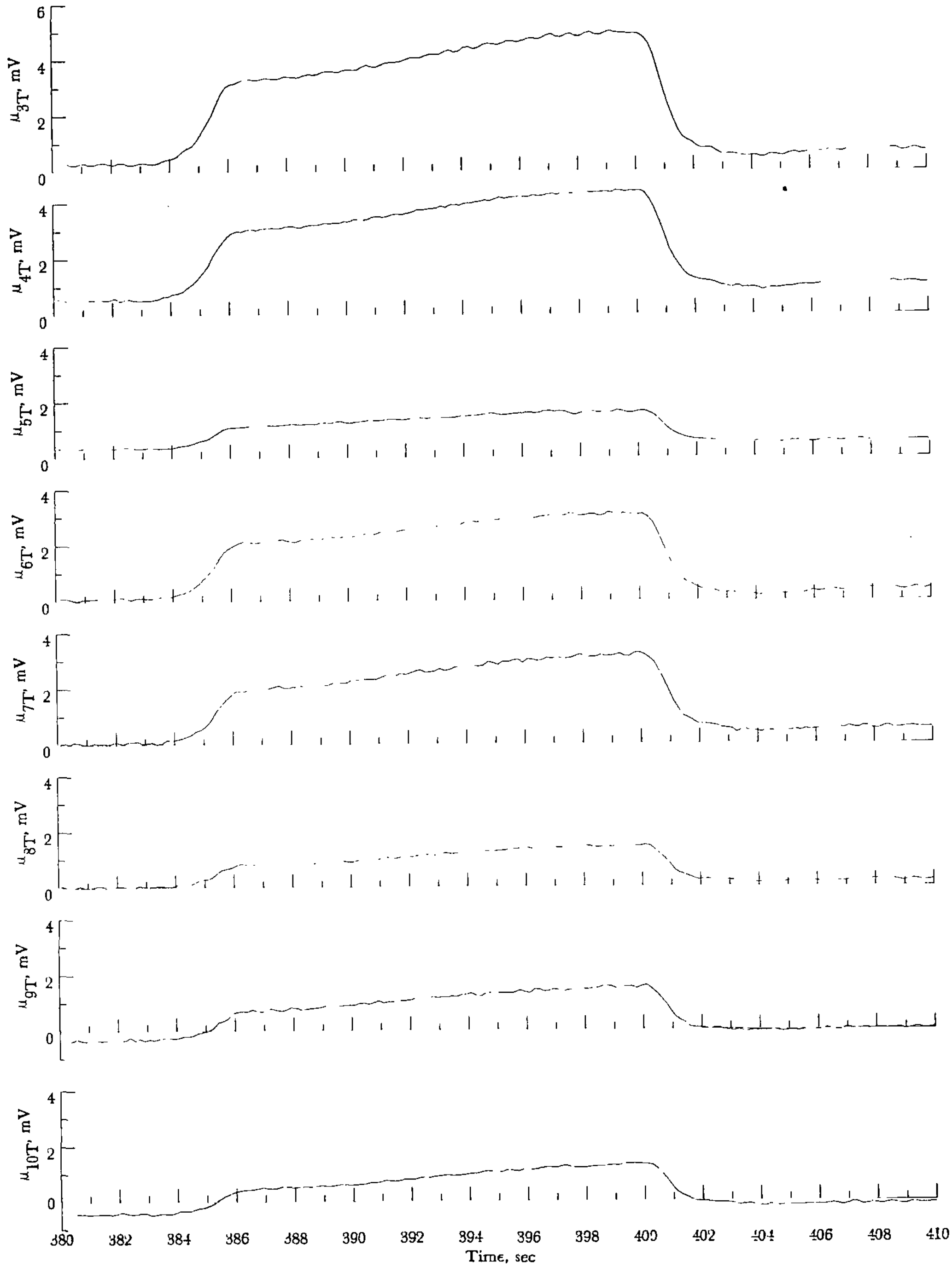

Figure 7.- Concluded.

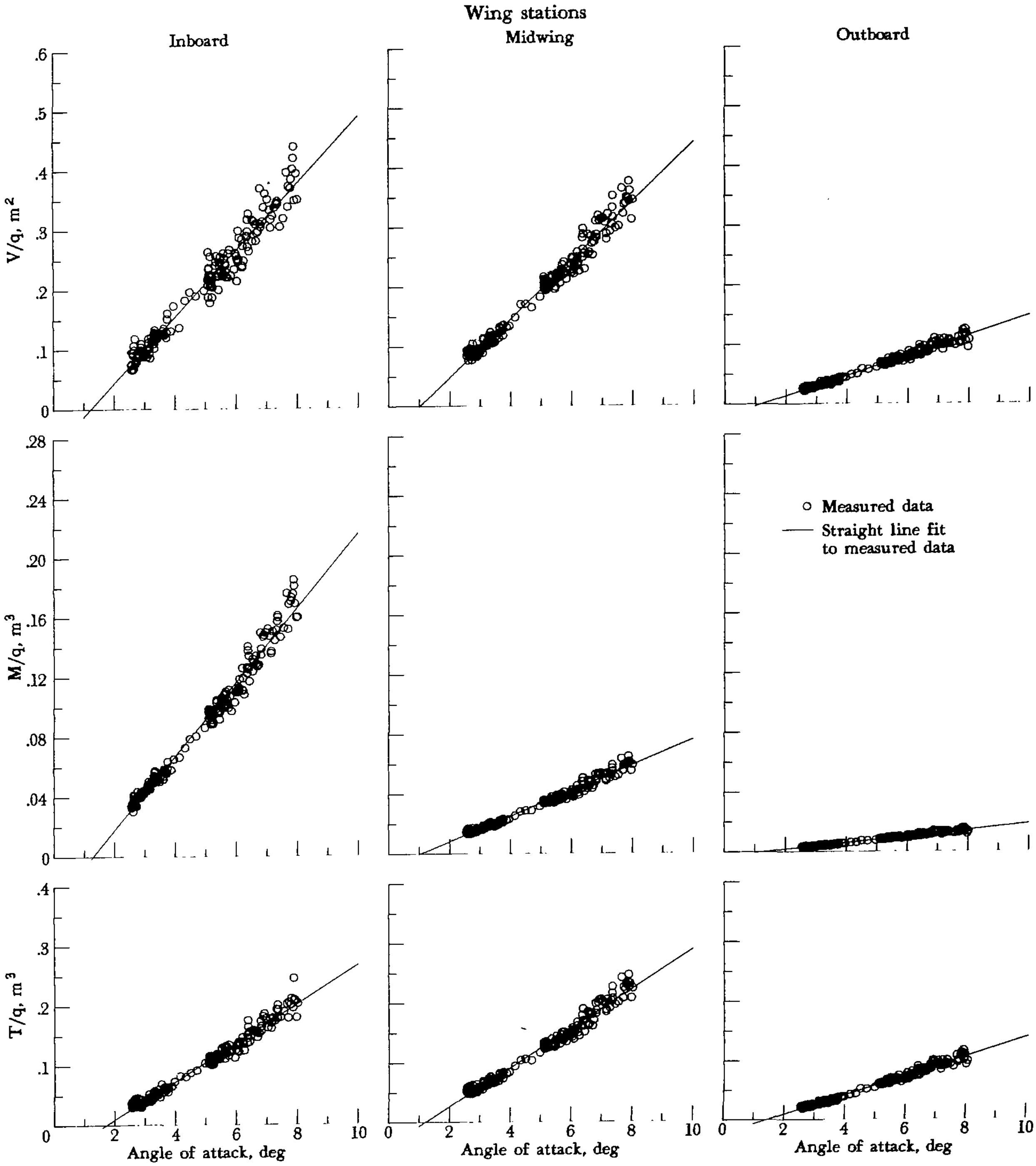

(a) Mach numbers 0.25 to 0.75; 7.5 kPa < q_∞ < 33.2 kPa; 174 samples.

Figure 8.- Flight-test measurements of wing structural loads for tank-on aircraft configuration.

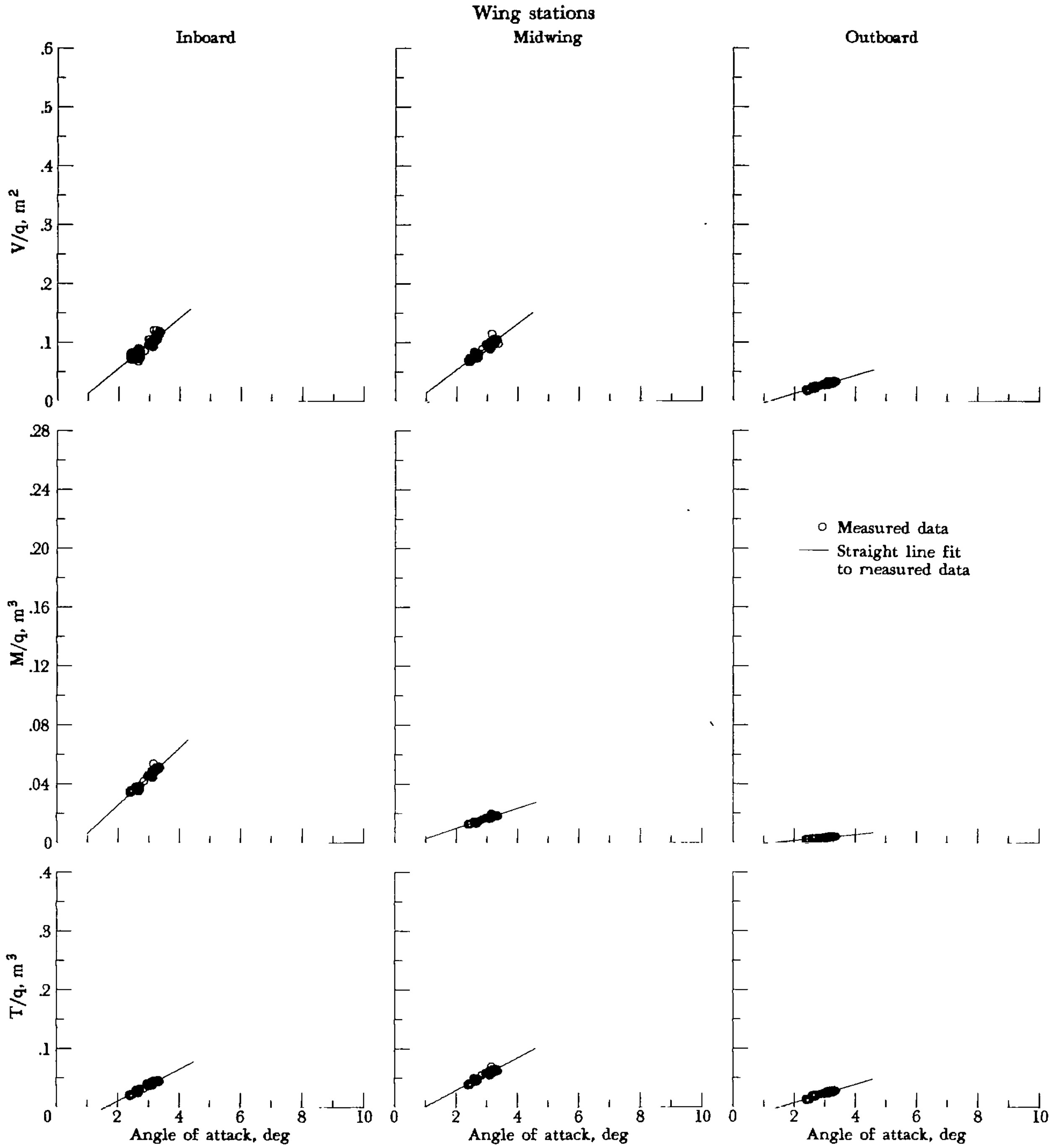

(b) Mach numbers 0.75 ± 0.025; 33.4 kPa < q_∞ < 40.0 kPa; 59 samples.

Figure 8.- Continued.

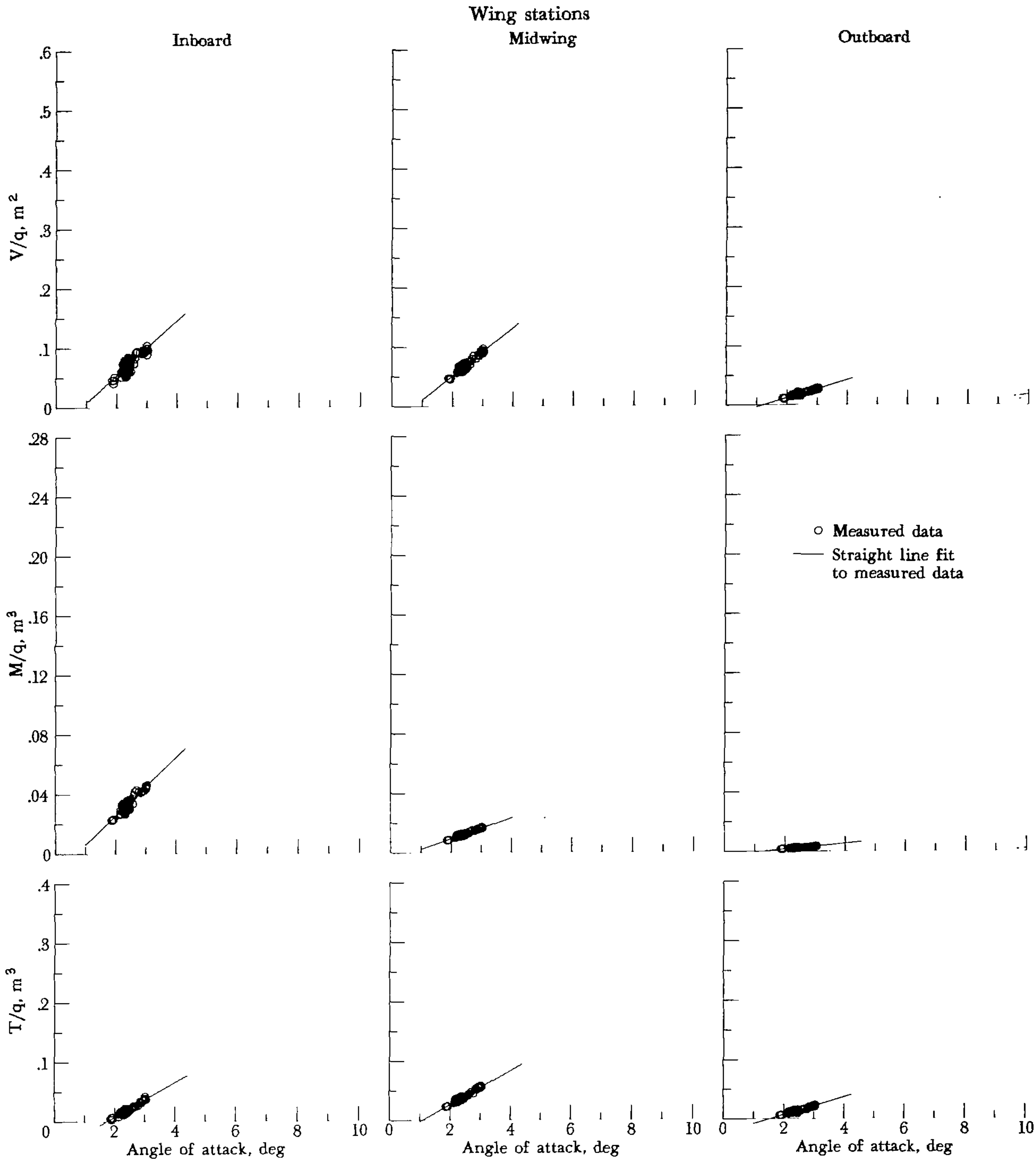

(c) Mach numbers 0.80 ± 0.025; 37.6 kPa < q_∞ < 45.0 kPa; 133 samples.

Figure 8.- Continued.

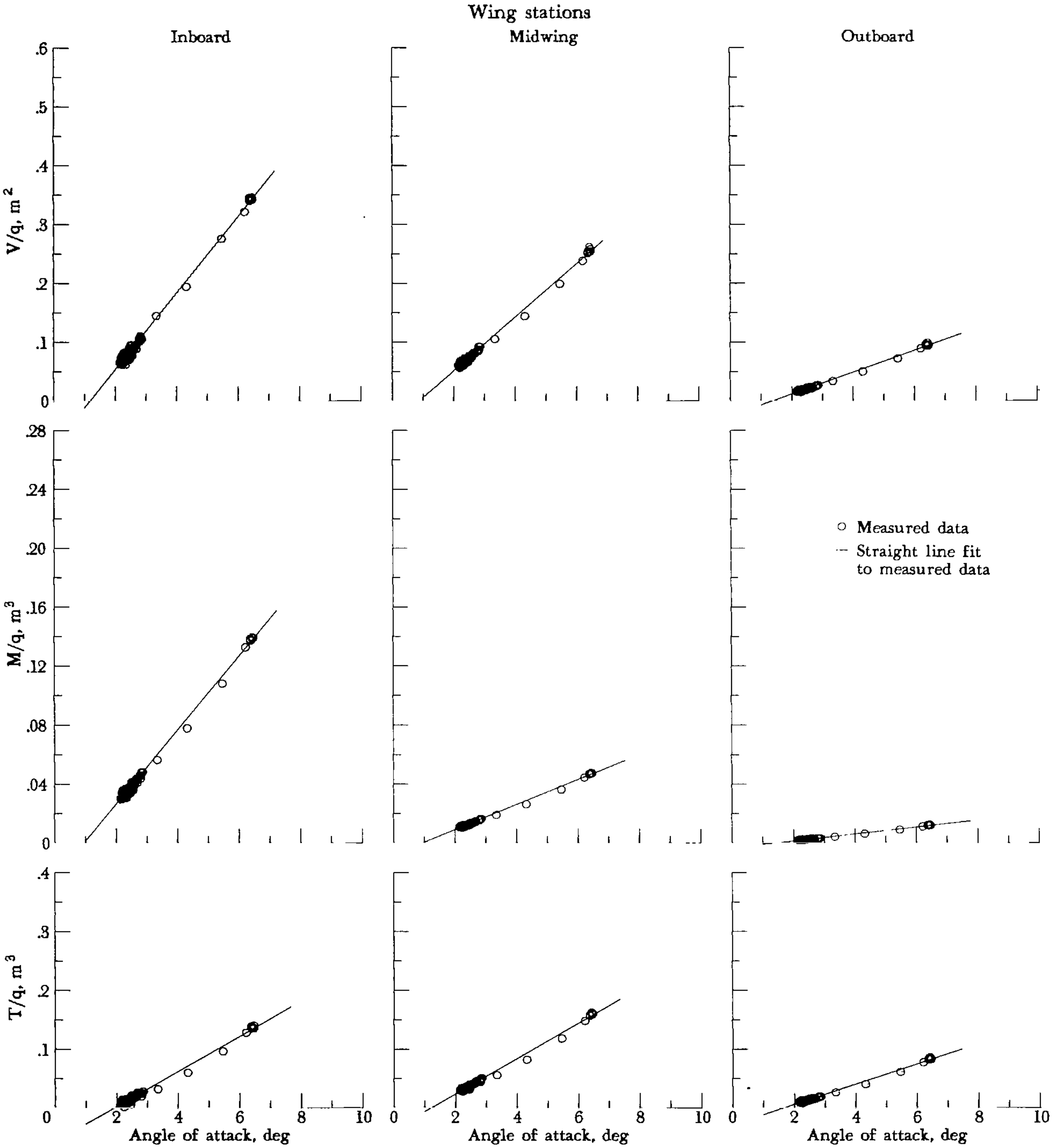

(d) Mach numbers 0.85 ± 0.025; 34.1 kPa < q_{∞} < 46.6 kPa; 108 samples.

Figure 8.- Continued.

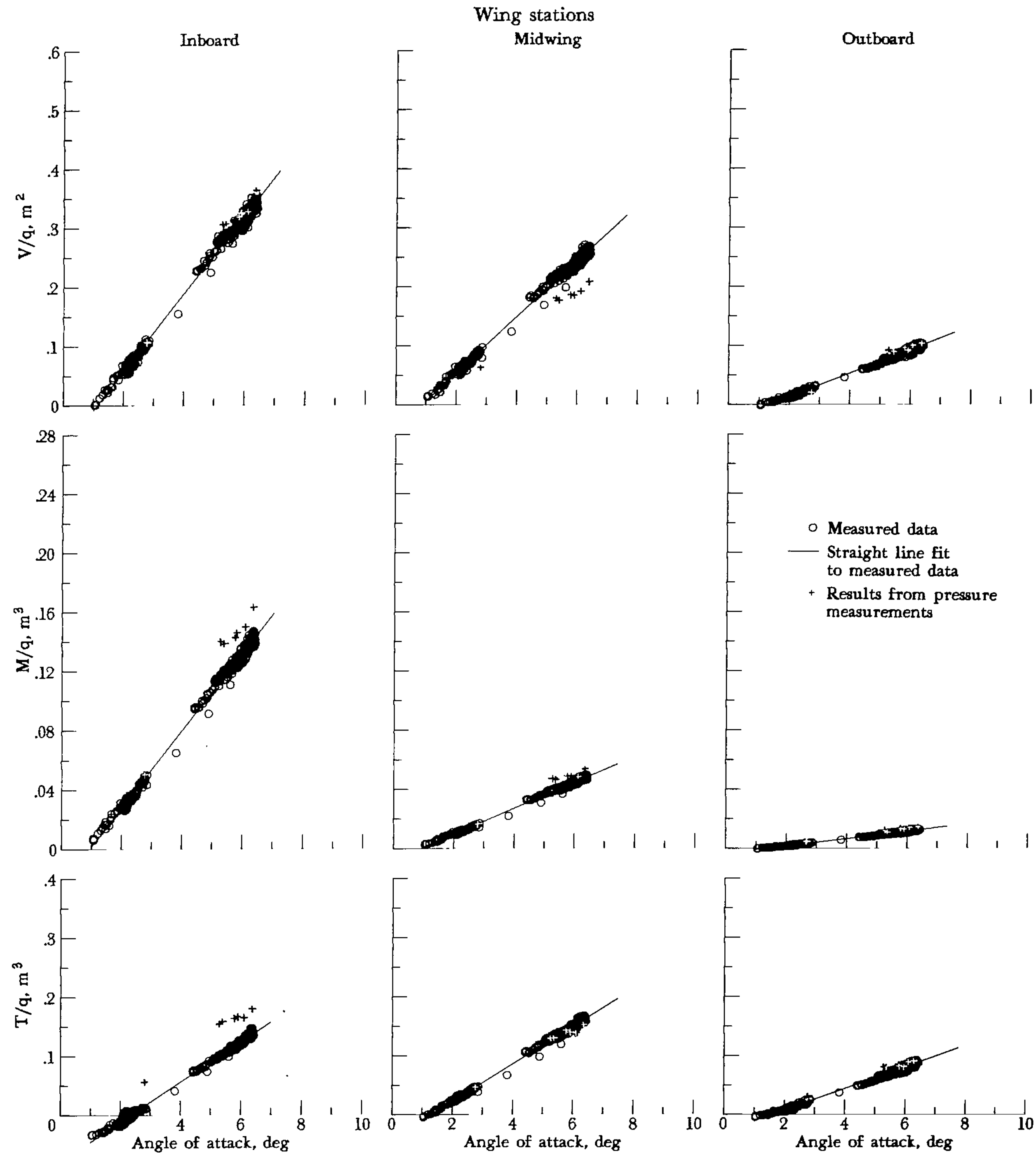

(e) Mach numbers 0.90 ± 0.025; 28.8 kPa < q_∞ < 51.0 kPa; 382 samples.

Figure 8.- Continued.

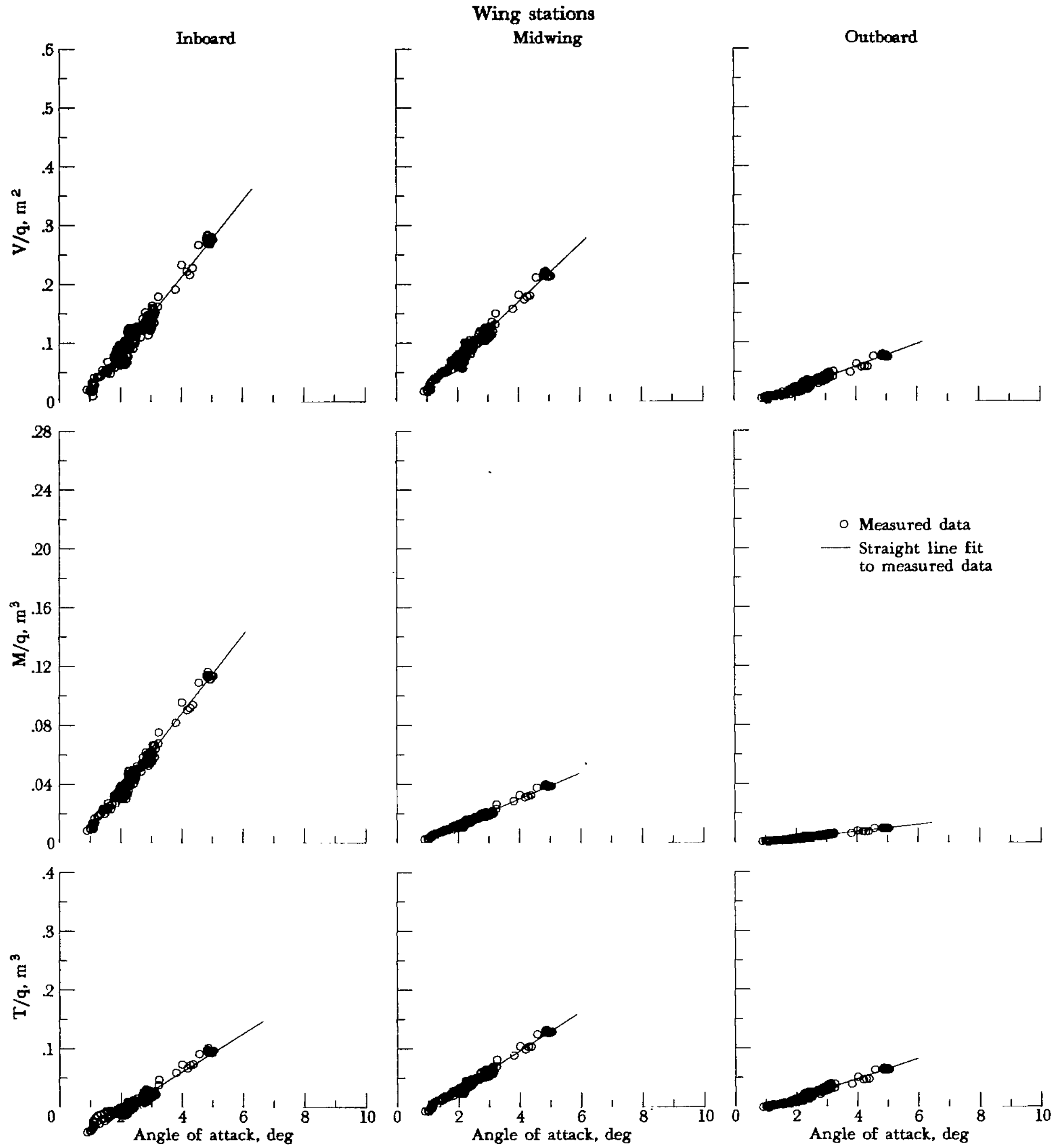

(f) Mach numbers 0.95 ± 0.025; 19.4 kPa < q_∞ < 52.3 kPa; 205 samples.

Figure 8.- Concluded.

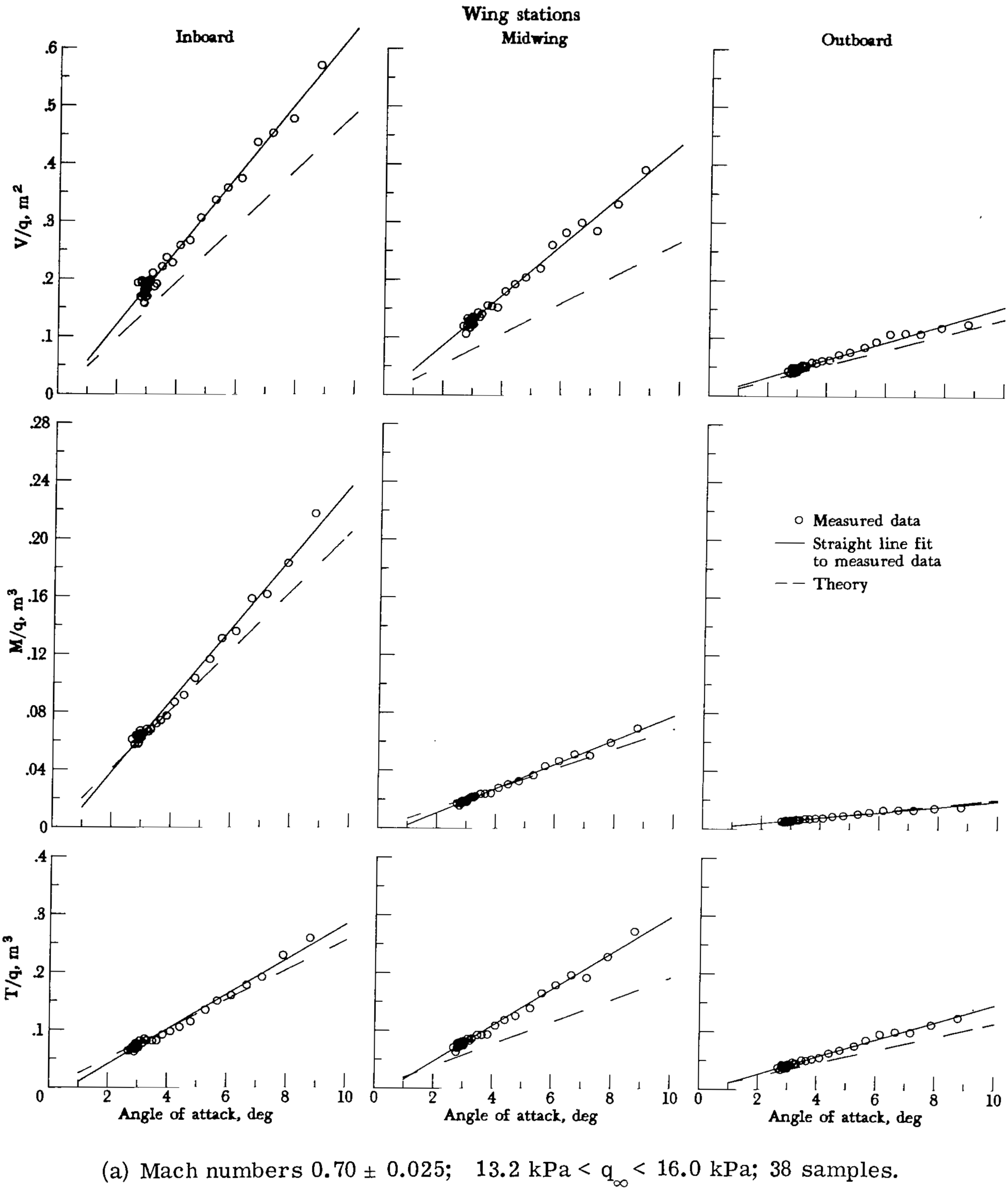

(a) Mach numbers 0.70 ± 0.025; 13.2 kPa < q_∞ < 16.0 kPa; 38 samples.

Figure 9.- Flight-test measurements of wing structural loads for the tank-off aircraft configuration.

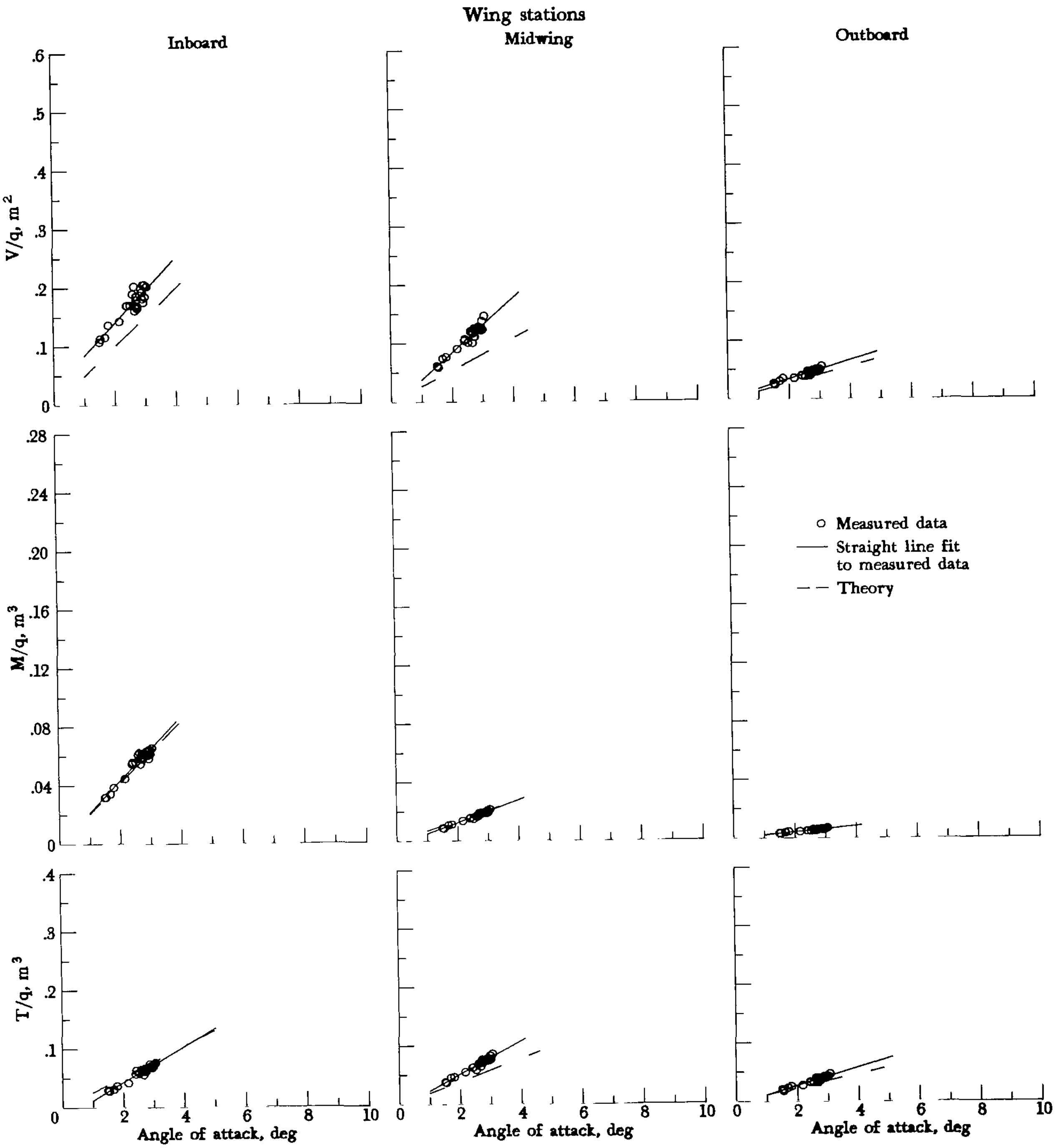

(b) Mach numbers 0.75 ± 0.025; 13.9 kPa < q_{∞} < 17.3 kPa; 24 samples.

Figure 9.- Continued.

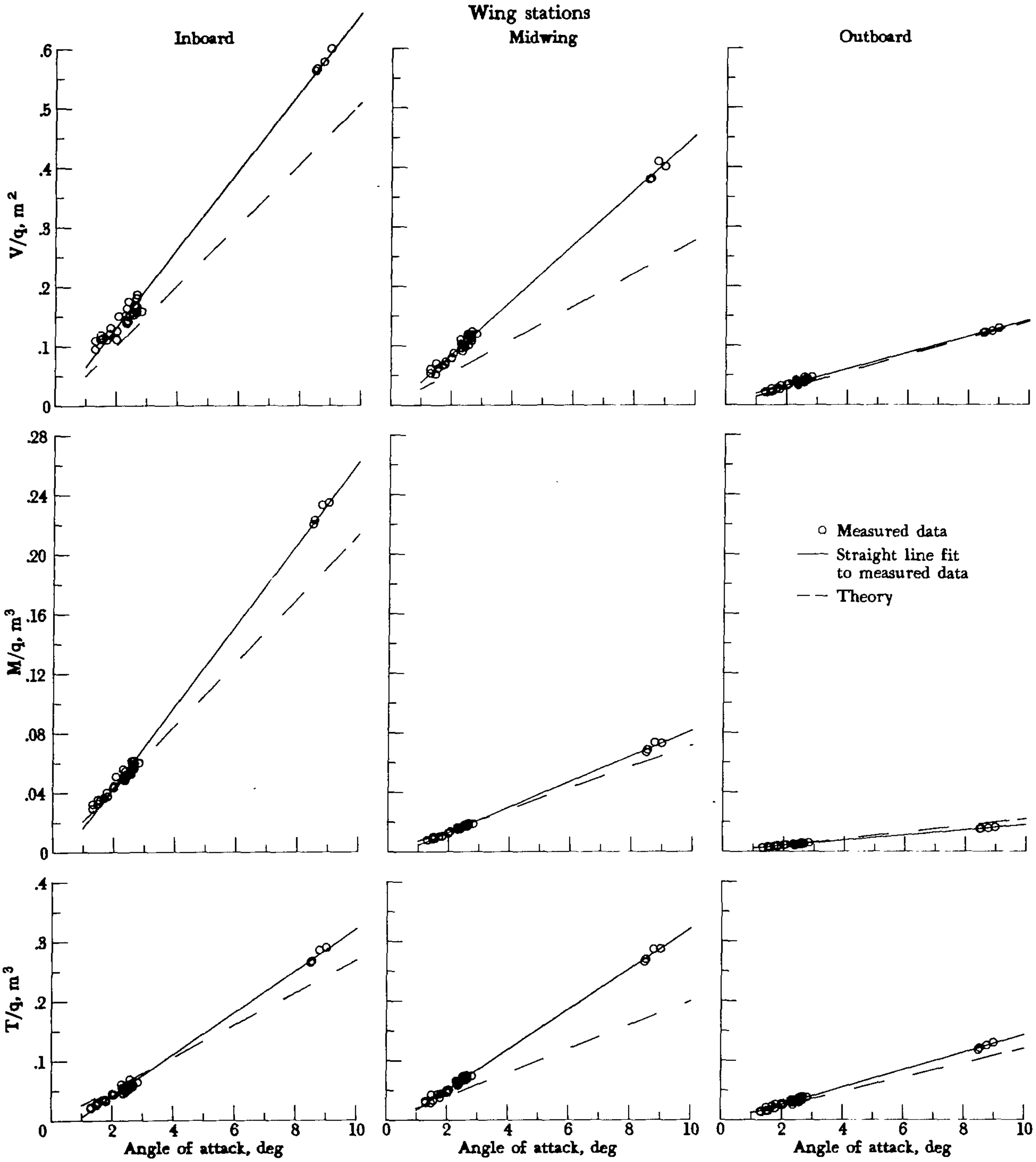

(c) Mach numbers 0.80 ± 0.025; 15.1 kPa < q_{∞} < 21.1 kPa; 32 samples.

Figure 9.- Continued.

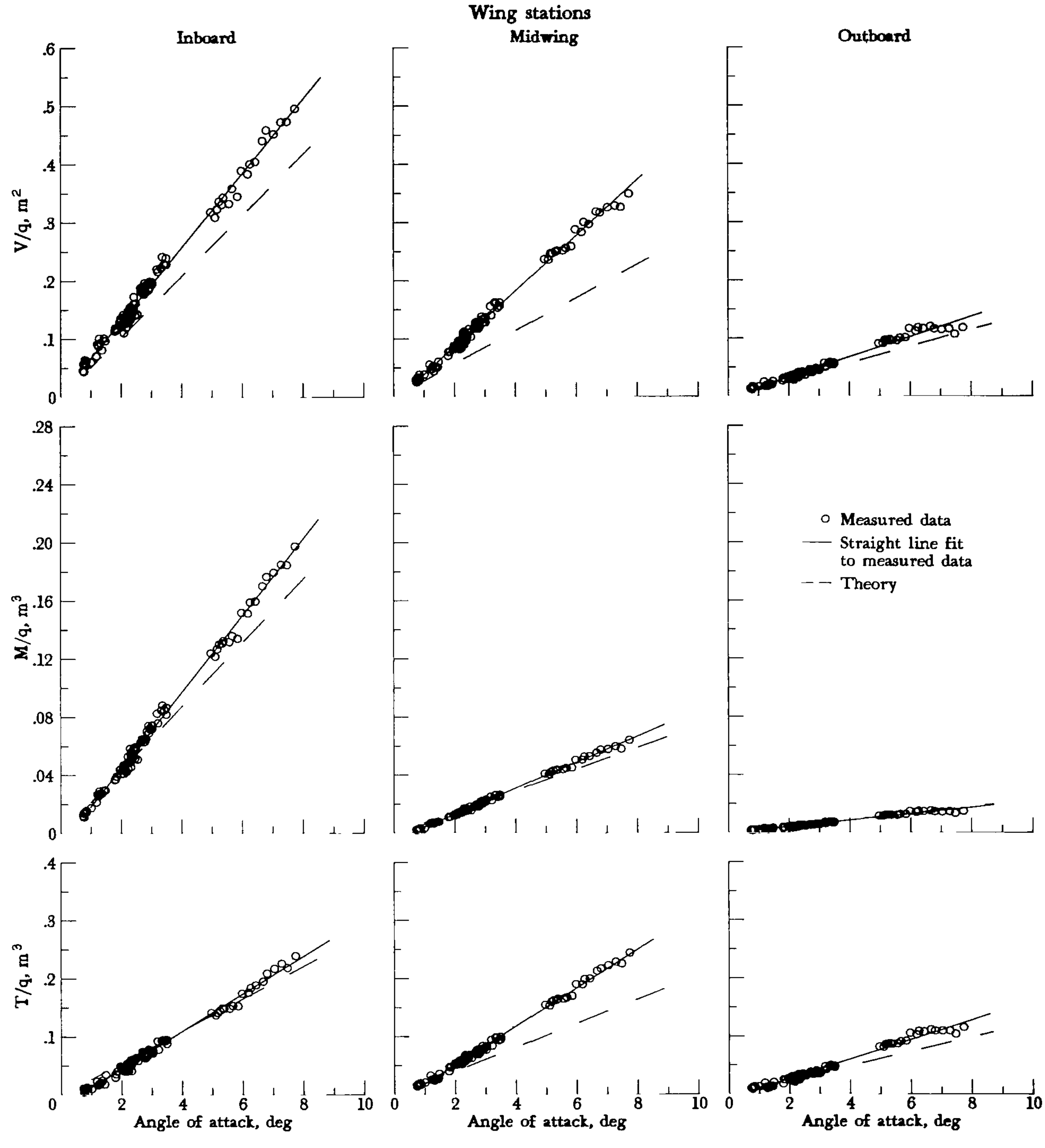

(d) Mach numbers 0.85 ± 0.025; 17.4 kPa < q_{∞} < 23.7 kPa; 97 samples.

Figure 9.- Continued.

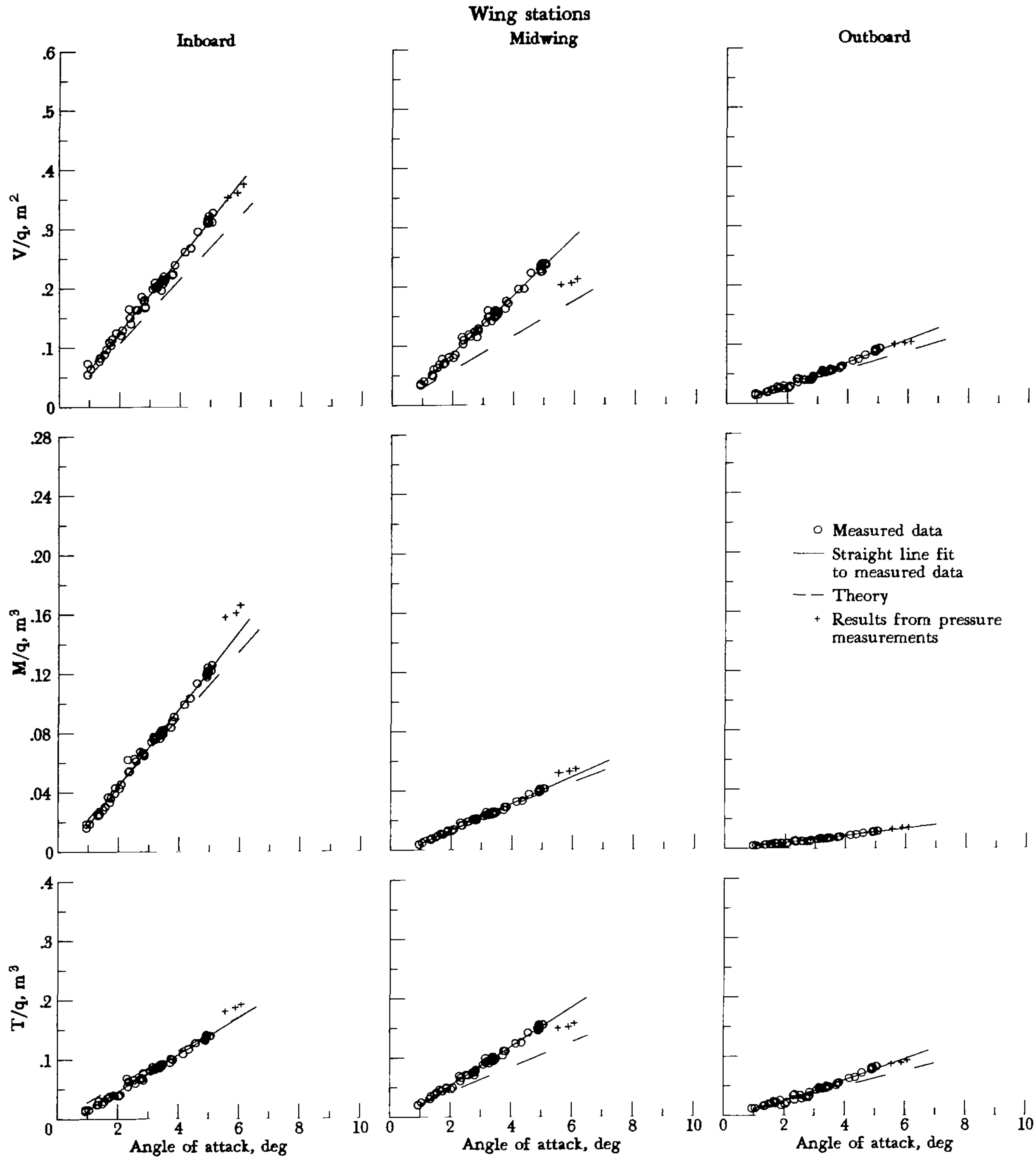

(e) Mach numbers 0.90 ± 0.025; 19.5 kPa < q_∞ < 23.9 kPa; 52 samples.

Figure 9.- Continued.

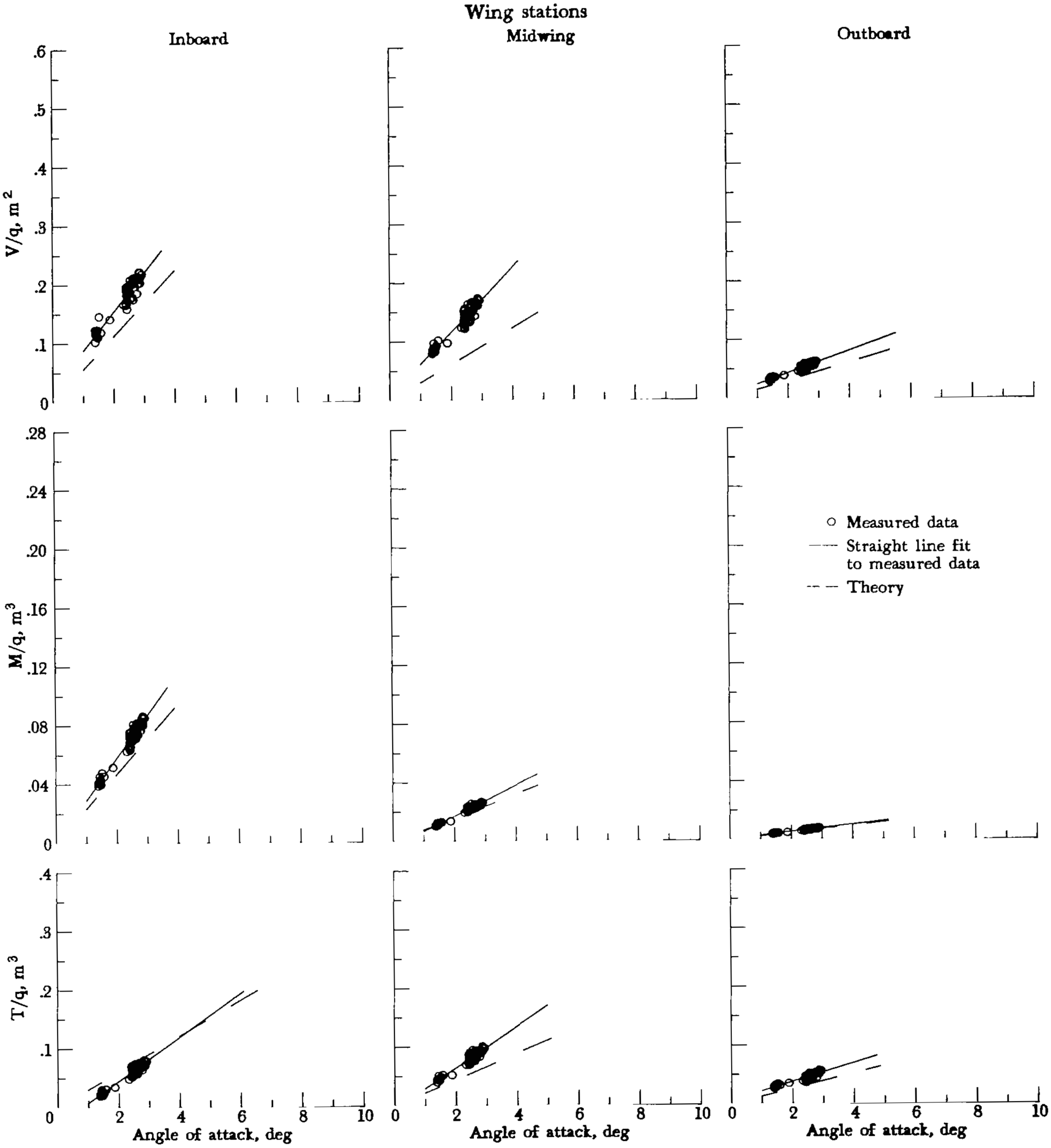

(f) Mach numbers 0.95 ± 0.025; 14.0 kPa < q_∞ < 19.7 kPa; 52 samples.

Figure 9.- Continued.

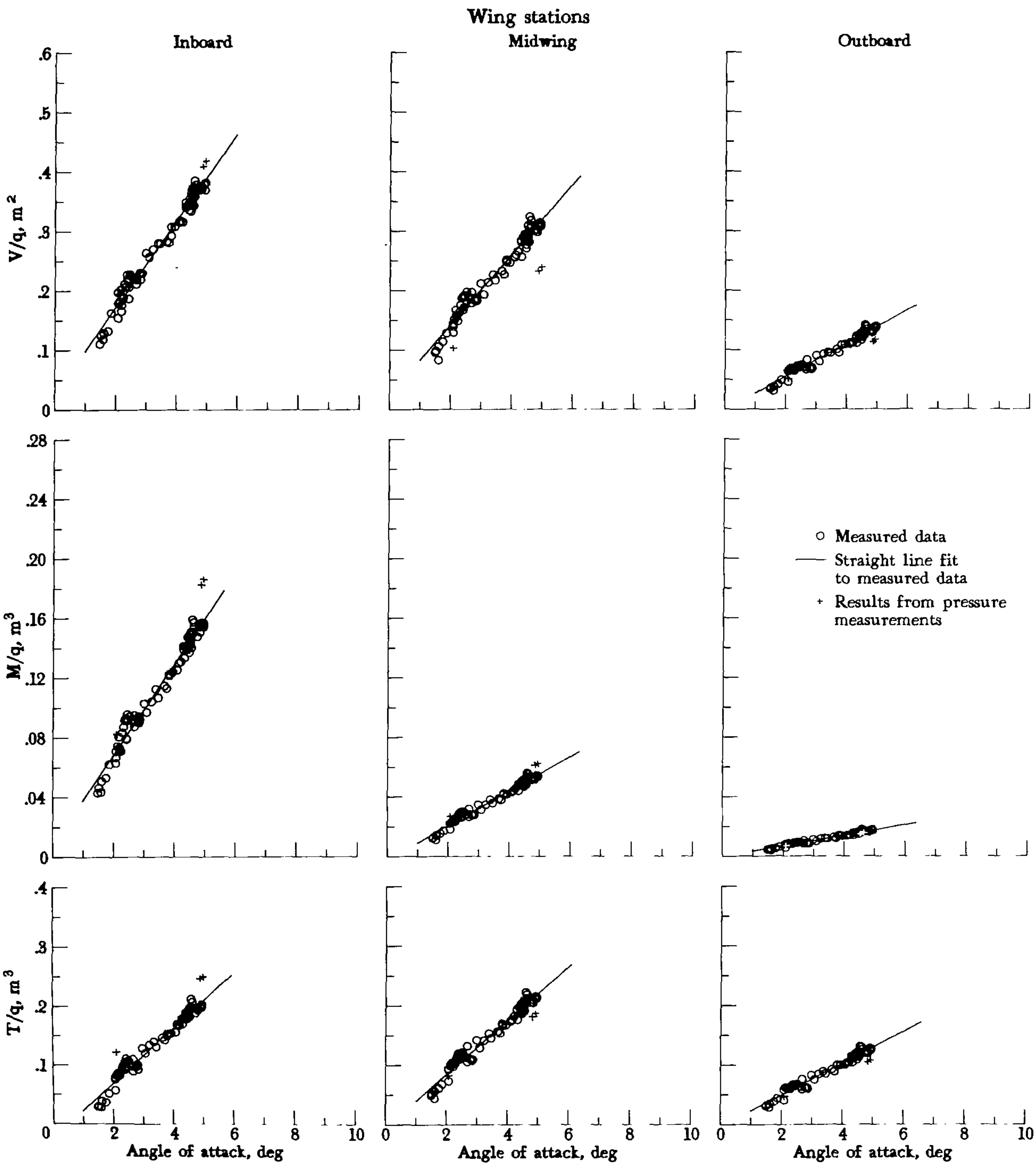

(g) Mach numbers 1.00 ± 0.025; 13.5 kPa < q_∞ < 18.5 kPa; 77 samples.

Figure 9.- Continued.

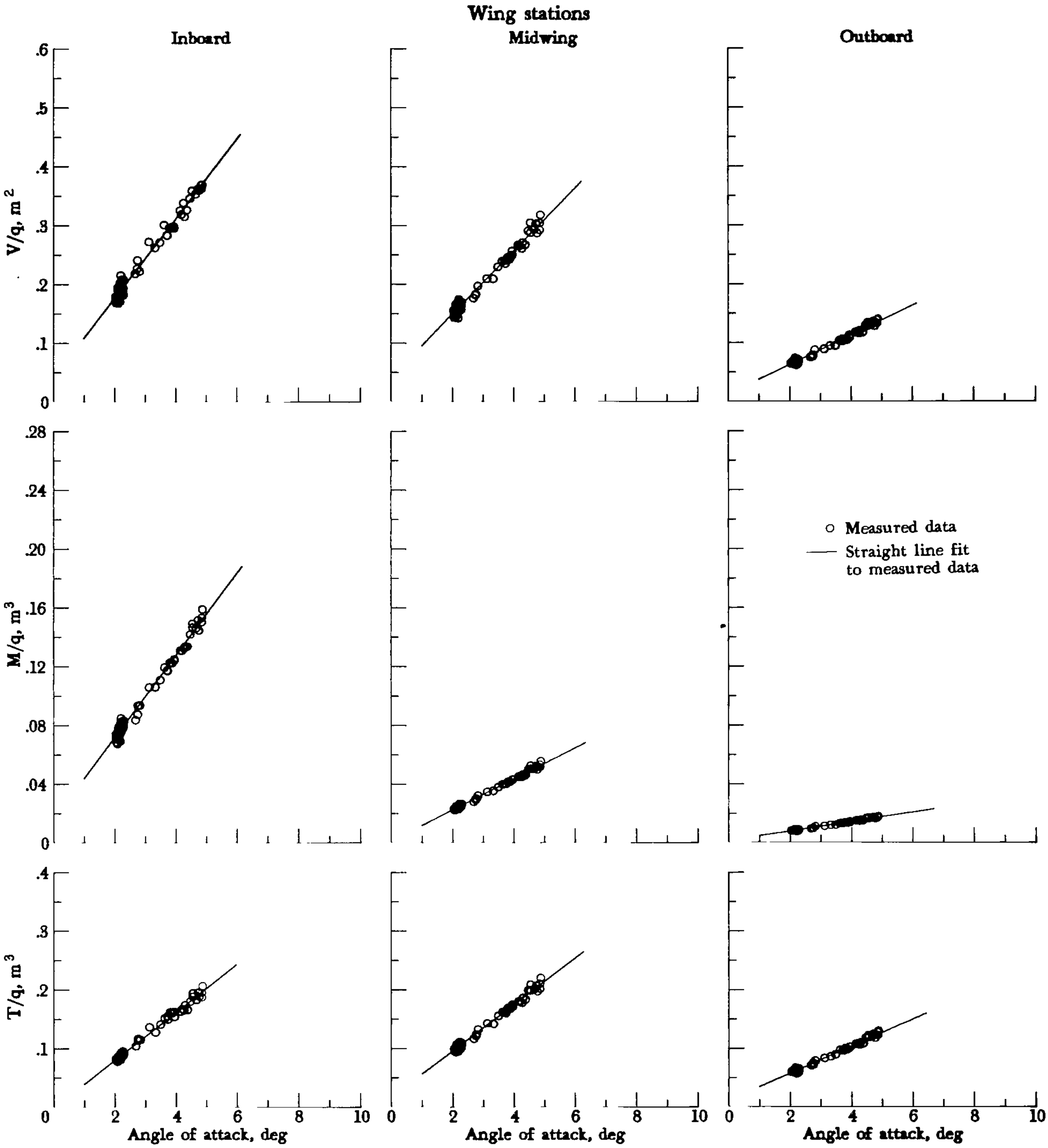

(h) Mach number 1.05 ± 0.025; 16.0 kPa < q_∞ < 19.2 kPa; 84 samples.

Figure 9.- Continued.

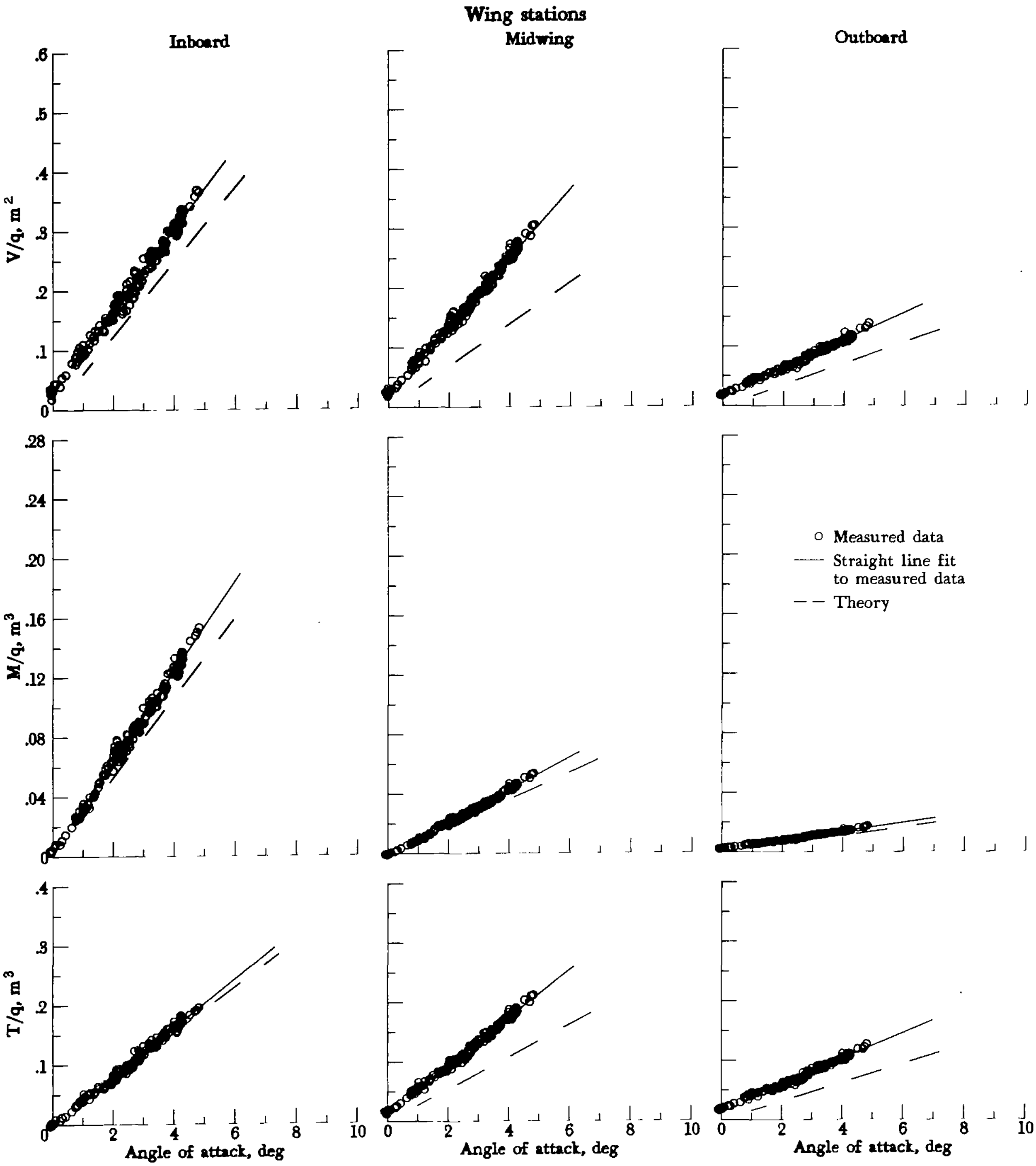

(i) Mach numbers 1.10 ± 0.025; 13.2 kPa < q_∞ < 21.5 kPa; 190 samples.

Figure 9.- Continued.

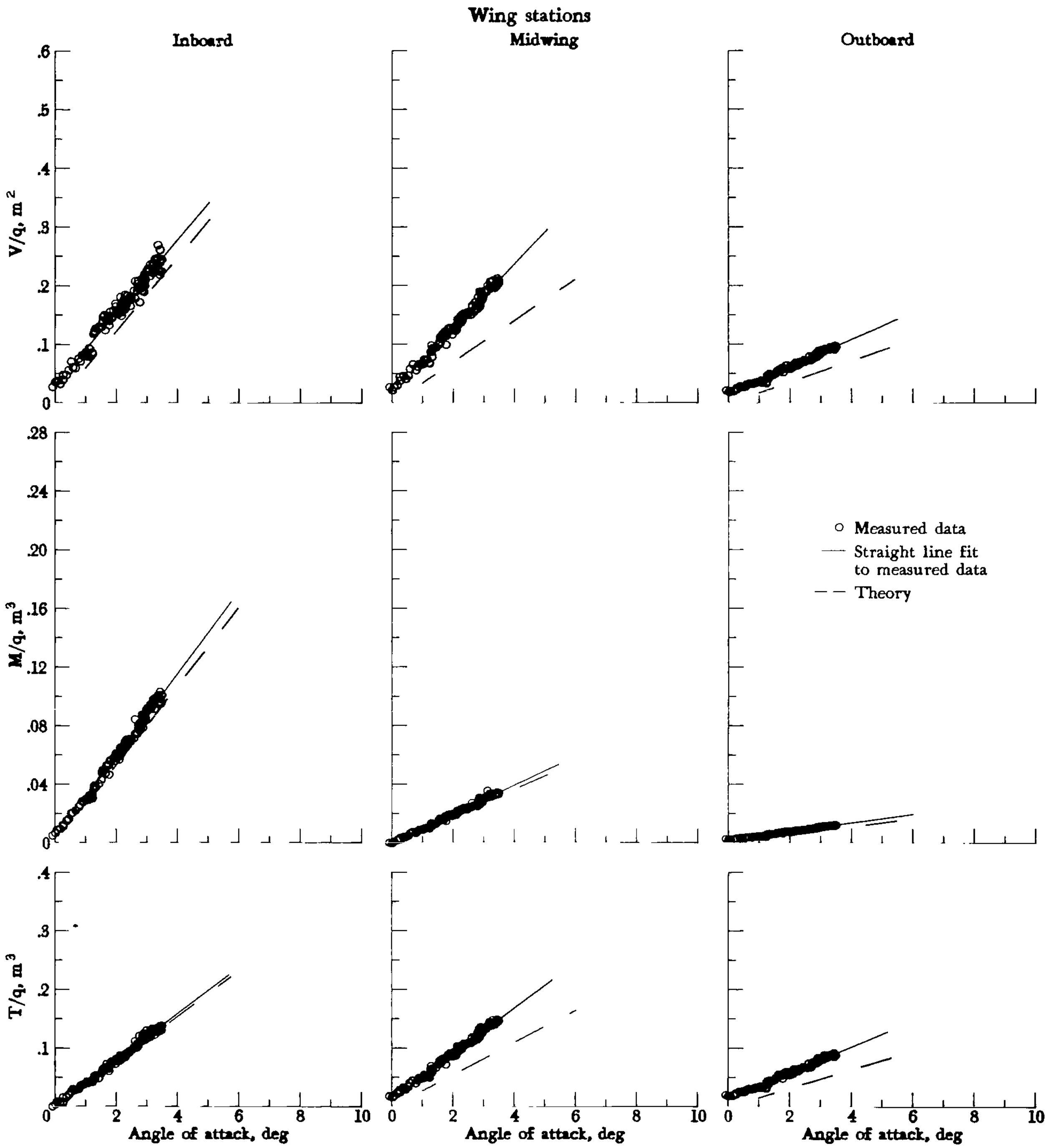

(j) Mach numbers 1.15 ± 0.025; 14.1 kPa < q_∞ < 23.2 kPa; 125 samples.

Figure 9.- Continued.

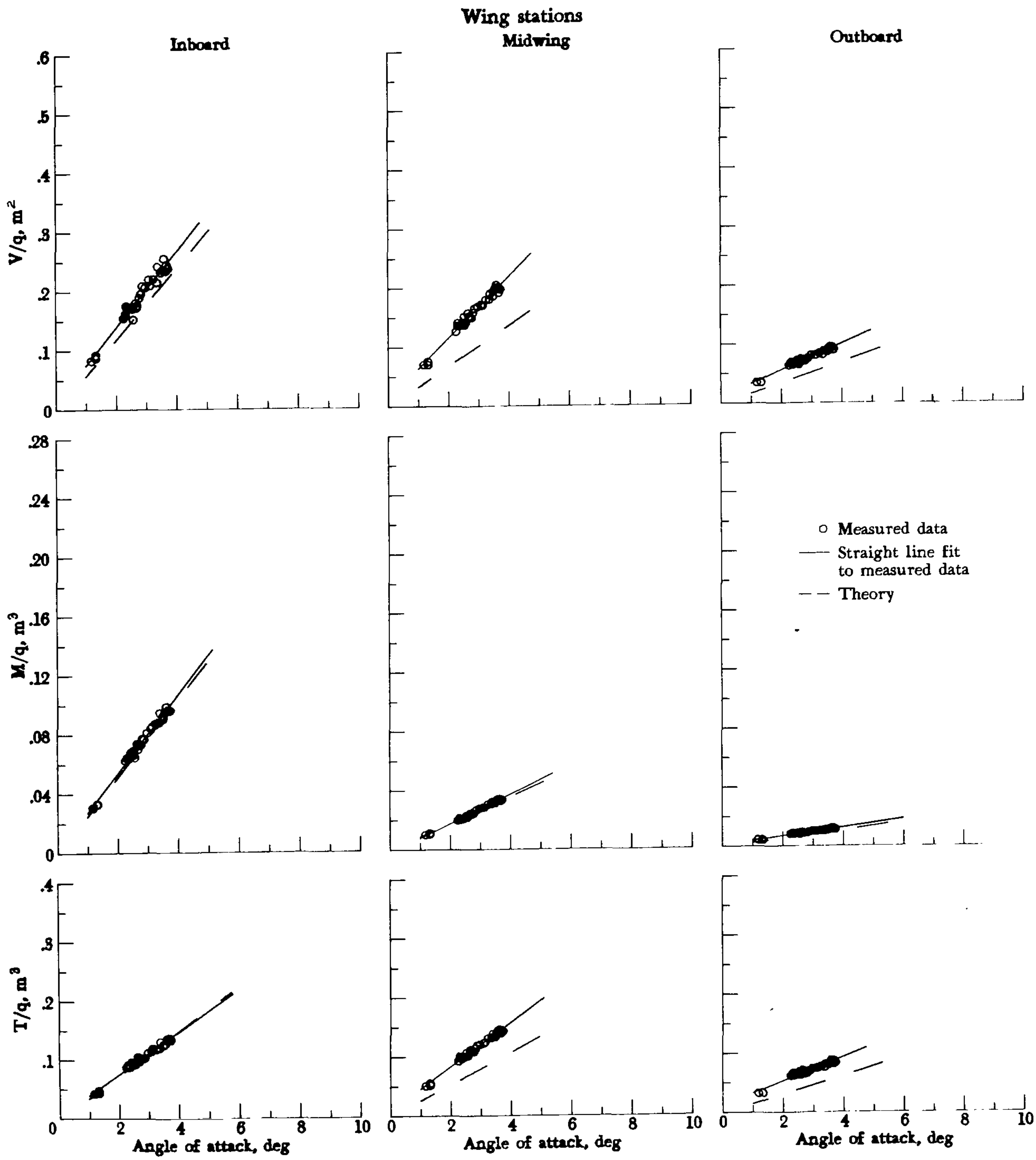

(k) Mach numbers 1.20 ± 0.025; 15.3 kPa < q_∞ < 23.8 kPa; 33 samples.

Figure 9.- Continued.

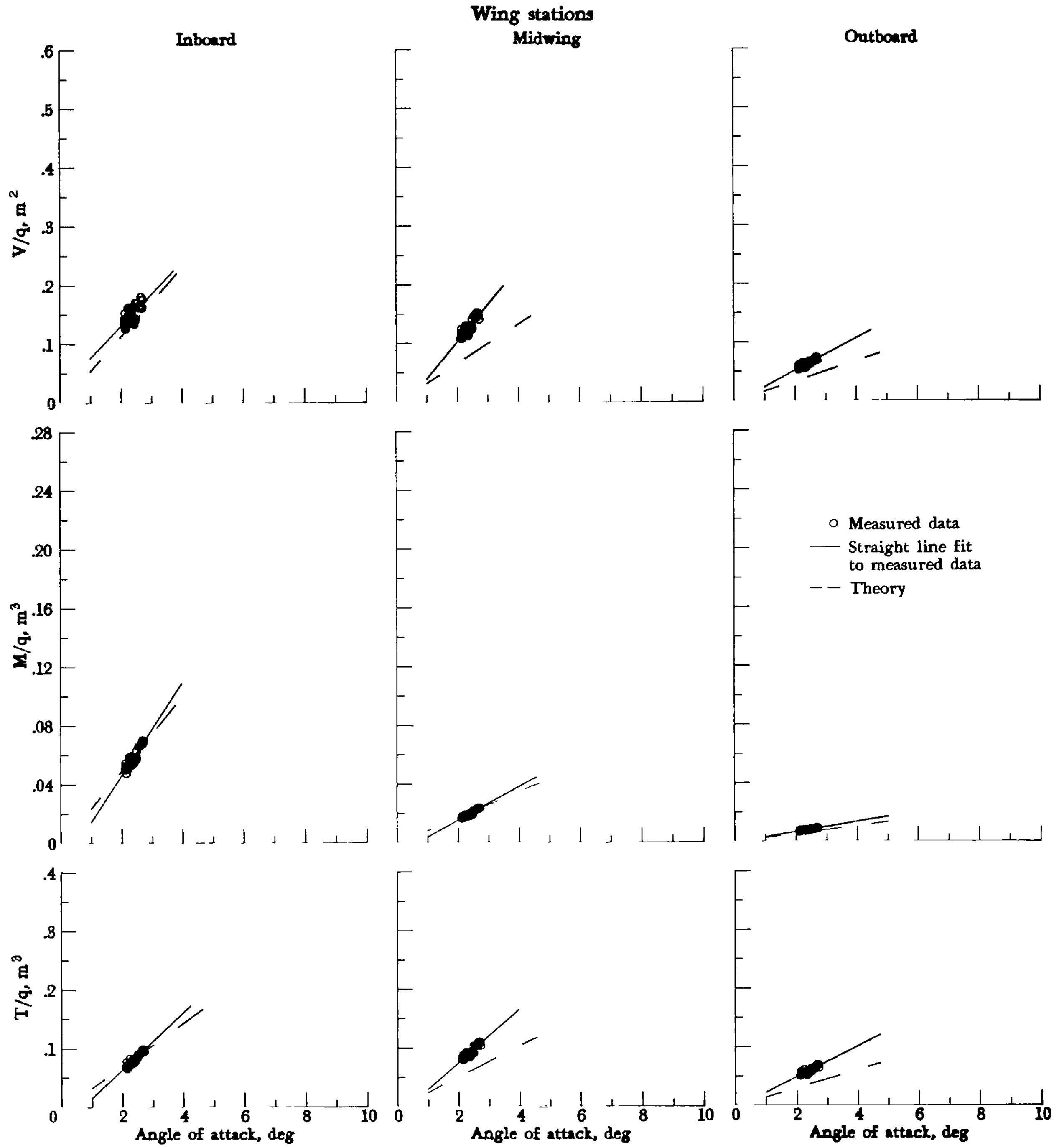

(l) Mach numbers 1.25 ± 0.025; 16.5 kPa < q_∞ < 20.3 kPa; 41 samples.

Figure 9.- Concluded.

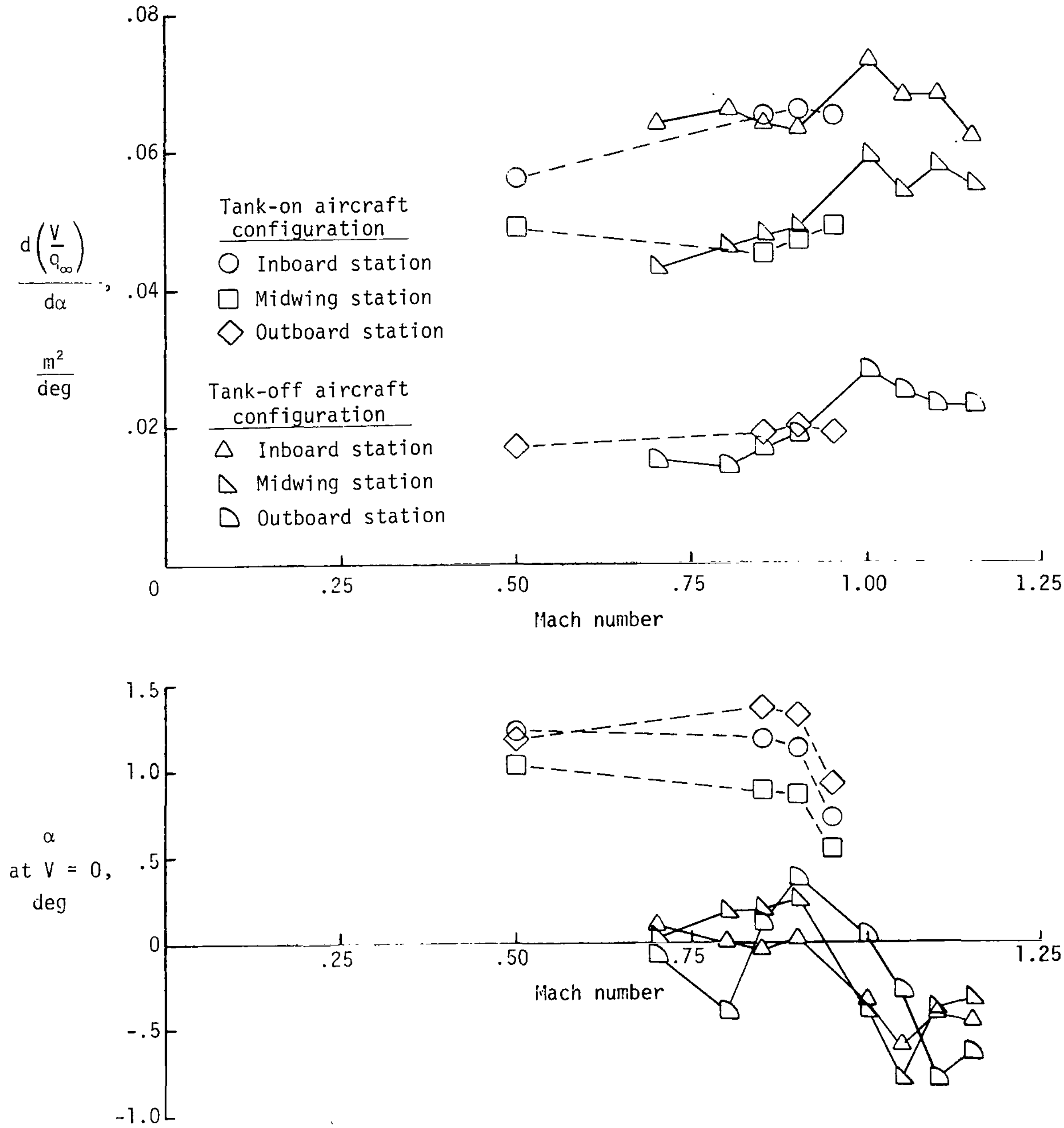

(a) Shear.

Figure 10.- Variation of wingload slope and intercept with Mach number.

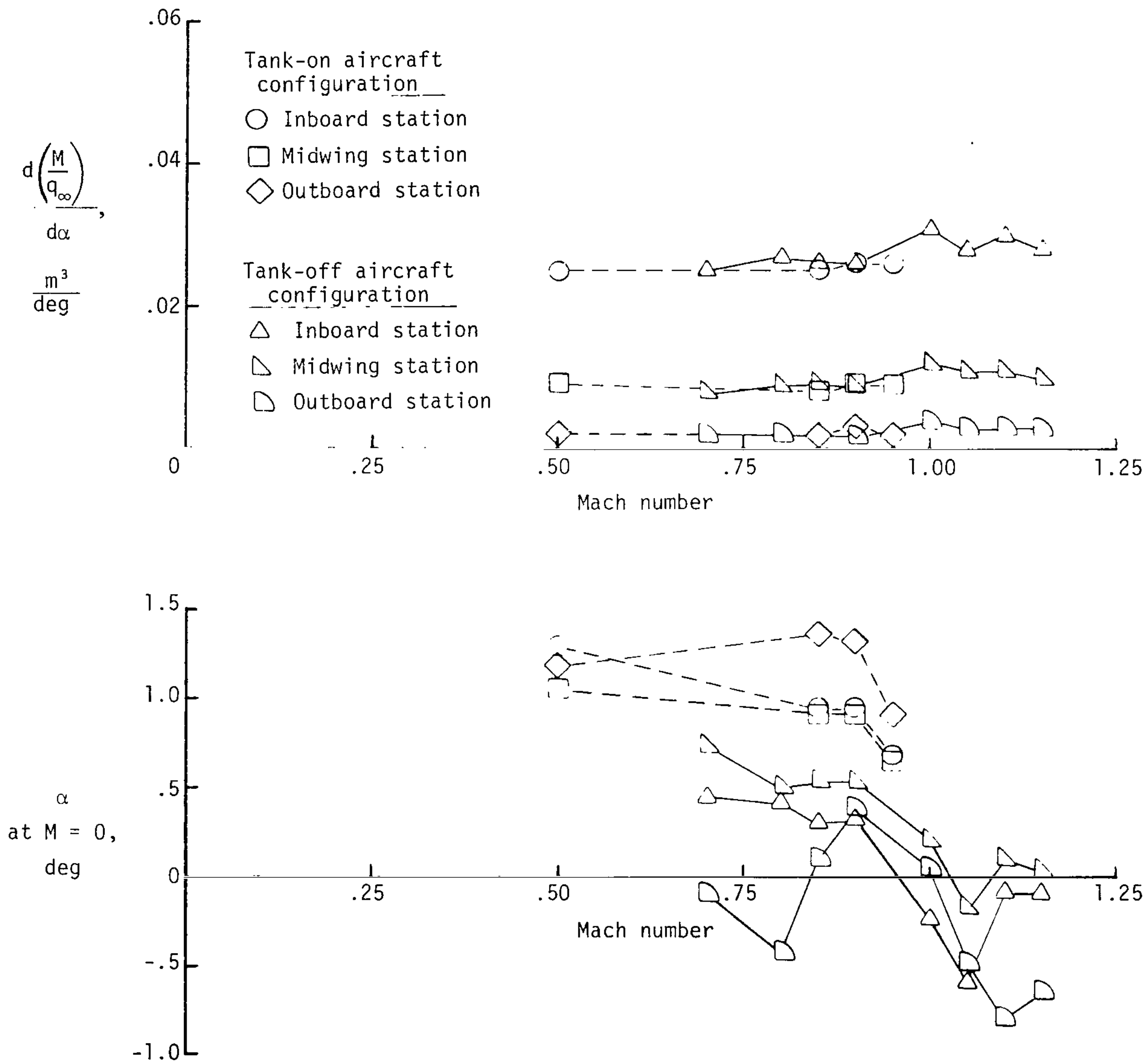

(b) Bending moment.

Figure 10.- Continued.

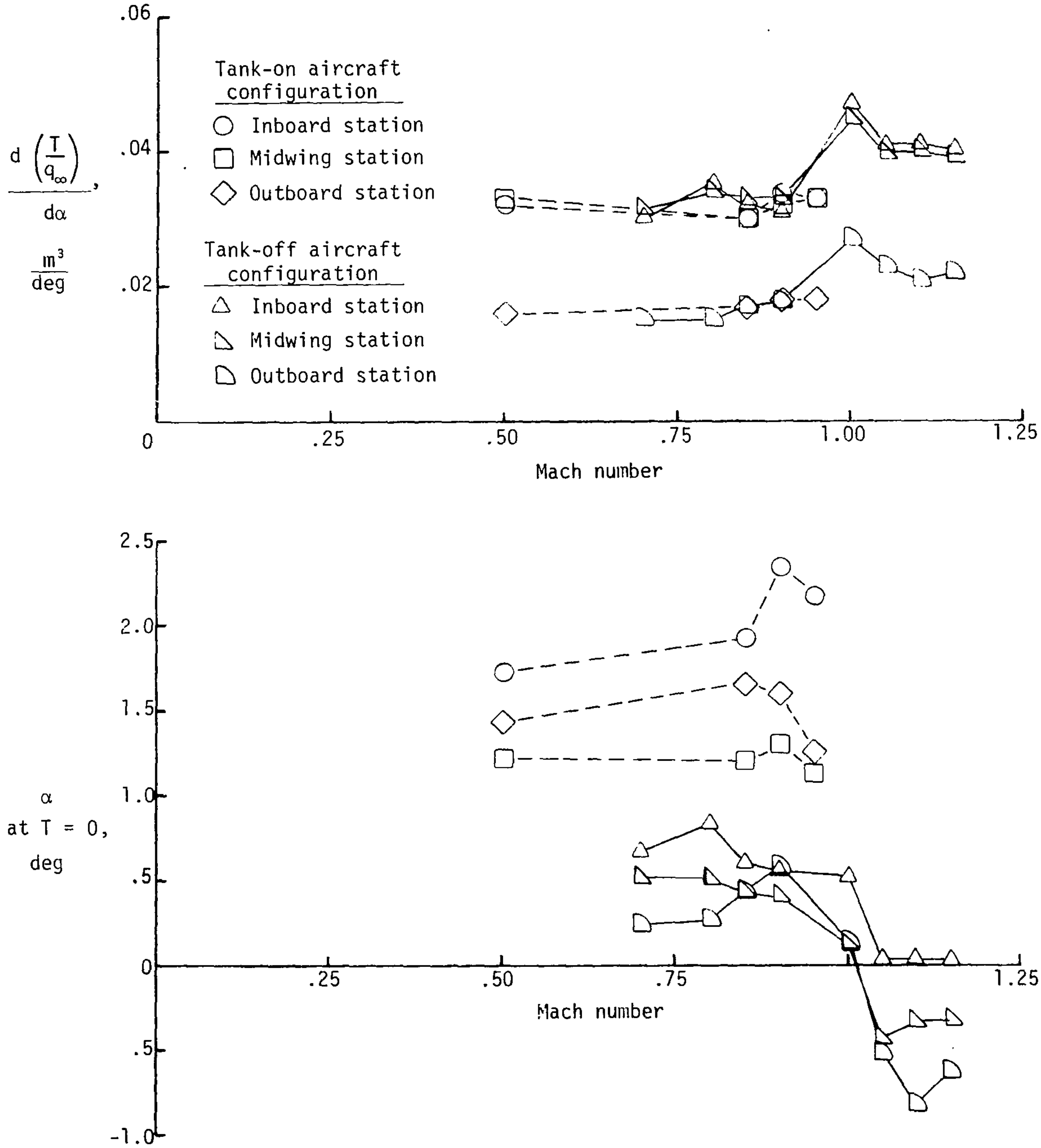

(c) Torsion.

Figure 10.- Concluded.

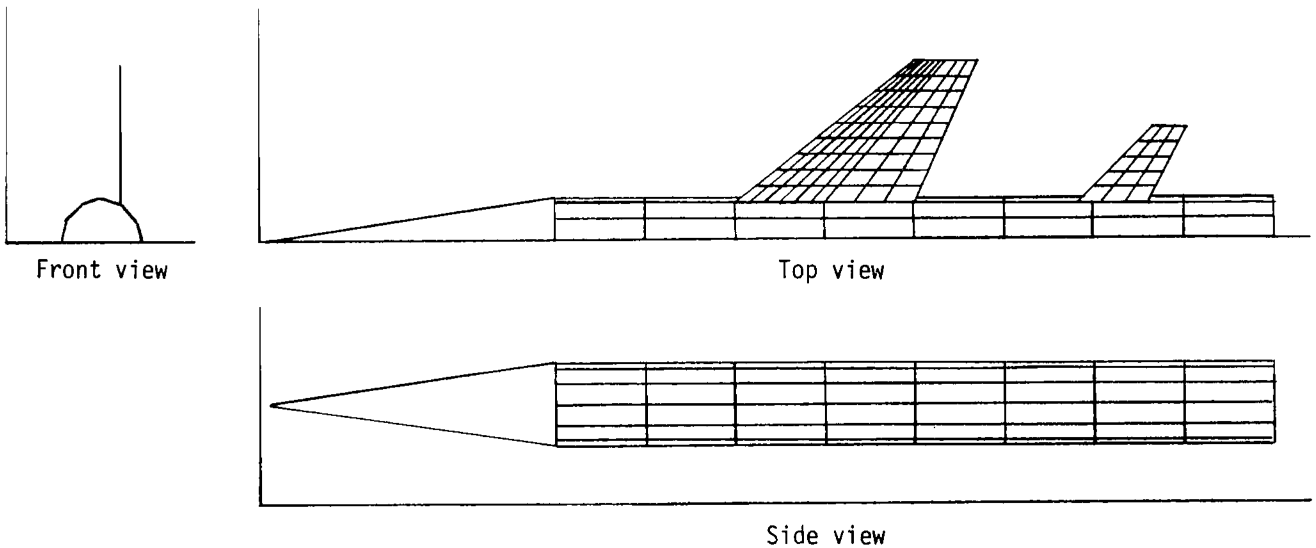

Figure 11.- Mathematical model of research vehicle.

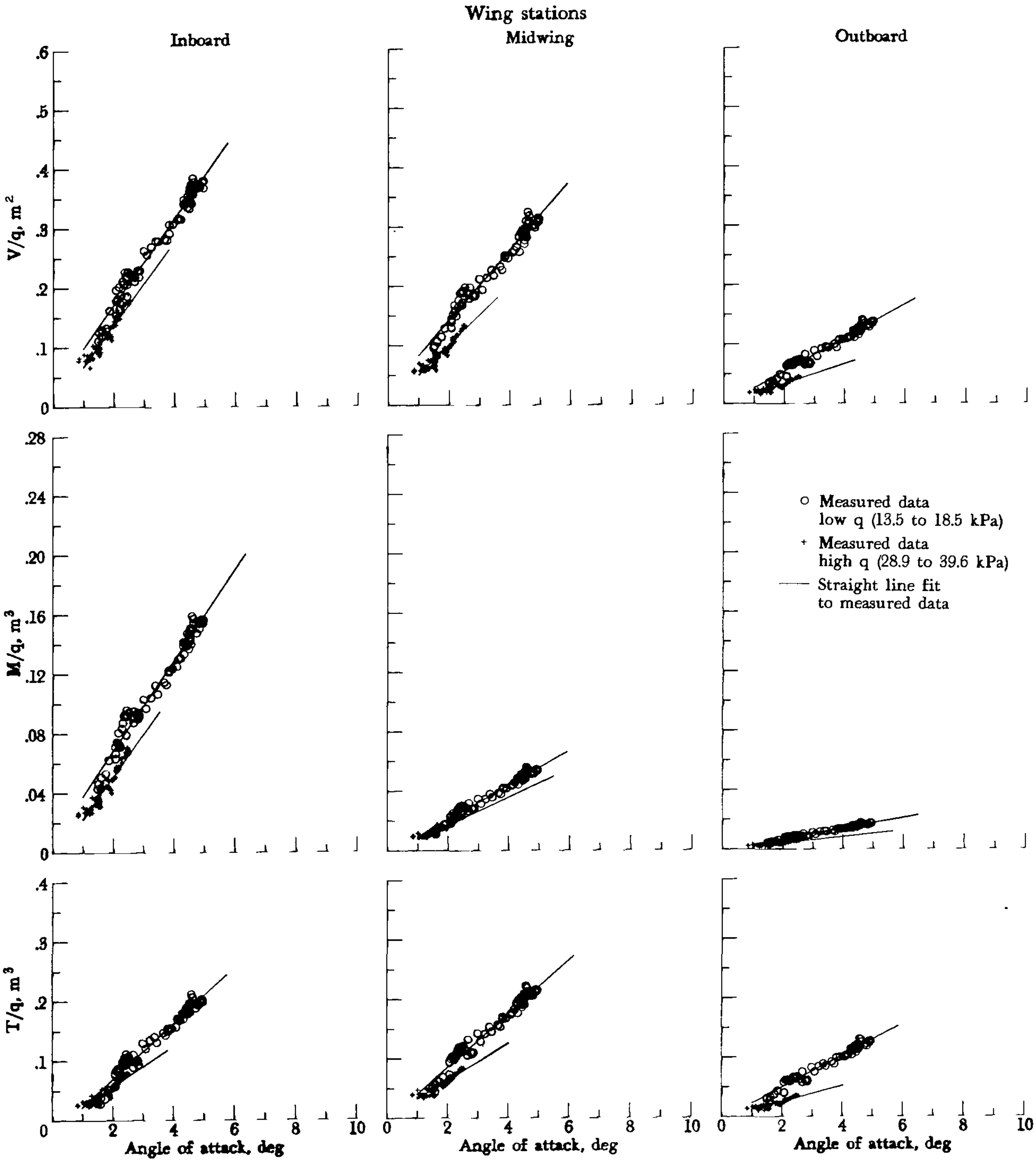

Figure 12.- Differences in wingloads for high and low levels of flight dynamic pressure, inboard station.

NASA-Langley, 1976 L-10904

"The aeronautical and space activities of the United States shall be conducted so as to contribute . . . to the expansion of human knowledge of phenomena in the atmosphere and space. The Administration shall provide for the widest practicable and appropriate dissemination of information concerning its activities and the results thereof."

—NATIONAL AERONAUTICS AND SPACE ACT OF 1958

NASA SCIENTIFIC AND TECHNICAL PUBLICATIONS

TECHNICAL REPORTS: Scientific and technical information considered important, complete, and a lasting contribution to existing knowledge.

TECHNICAL NOTES: Information less broad in scope but nevertheless of importance as a contribution to existing knowledge.

TECHNICAL MEMORANDUMS: Information receiving limited distribution because of preliminary data, security classification, or other reasons. Also includes conference proceedings with either limited or unlimited distribution.

CONTRACTOR REPORTS: Scientific and technical information generated under a NASA contract or grant and considered an important contribution to existing knowledge.

TECHNICAL TRANSLATIONS: Information published in a foreign language considered to merit NASA distribution in English.

SPECIAL PUBLICATIONS: Information derived from or of value to NASA activities. Publications include final reports of major projects, monographs, data compilations, handbooks, sourcebooks, and special bibliographies.

TECHNOLOGY UTILIZATION PUBLICATIONS: Information on technology used by NASA that may be of particular interest in commercial and other non-aerospace applications. Publications include Tech Briefs, Technology Utilization Reports and Technology Surveys.

Details on the availability of these publications may be obtained from:

SCIENTIFIC AND TECHNICAL INFORMATION OFFICE

NATIONAL AERONAUTICS AND SPACE ADMINISTRATION

Washington, D.C. 20546